The Etv1/Er81 transcription factor coordinates myelination-related genes to regulate Schwann cell differentiation and myelination

Parizat Askar[#], Jinghui Xu[#], Junxia Hu, Jianghong Shangguan, Hualin Sun, Songlin Zhou, Xiaoming Yang, Gang Chen, Wenfeng Su, Yun Gu^

Jiangsu Key Laboratory of Neuroregeneration, Co-innovation Center of Neuroregeneration, Jiangsu Clinical Medicine Center of Tissue Engineering and Nerve Injury Repair, Nantong University, Nantong, China

Contributions: (I) Conception and design: Y Gu, W Su; (II) Administrative support: Y Gu, W Su; (III) Provision of study materials or patients: P Askar, J Xu, J Hu, J Shangguan; (IV) Collection and assembly of data: H Sun, S Zhou, X Yang; (V) Data analysis and interpretation: G Chen, W Su, Y Gu; (VI) Manuscript writing: All authors; (VII) Final approval of manuscript: All authors.

[#]These authors contributed equally to this work.

Correspondence to: Yun Gu; Wenfeng Su. Jiangsu Key Laboratory of Neuroregeneration, Co-innovation Center of Neuroregeneration, Jiangsu Clinical Medicine Center of Tissue Engineering and Nerve Injury Repair, Nantong University, Nantong 226001, China. Email: guyun@ntu.edu.cn; suwenfeng@ntu.edu.cn.

Background: Axonal myelination is critical for the functioning of vertebrate nervous system. Myelin sheath malformation or degeneration can cause a variety of neurological diseases. Our previous study identified multiple potential myelination-related transcriptional factors (TFs), including expressed sequence tag (ETS) variant transcription factor 1 (Etv1)/Er81, via gene microarray analysis of Schwann cells (SCs) at various myelination stages. Etv1 is known to be involved in the regulation of neuronal specialization, muscle spindle differentiation, and sensorimotor connectivity. However, to our knowledge, to date, there are no relevant studies that Etv1 regulates SC myelination.

Methods: To investigate the roles of Etv1 in SC re-myelination, an *in vivo* mouse myelination model was used, in which the sciatic nerve is crushed. Etv1 in nerves was knocked down via *in situ* injection of cholesterol-modified Etv1-small interfering (si)RNA. The expression of myelin-associated glycoprotein (MAG) was evaluated by Western blotting (WB) and immunohistochemistry (IHC). Myelination was assessed by transmission electron microscopy (TEM). The effects of Etv1 on SC proliferation, migration, and differentiation were assessed *in vitro* using the EdU cell proliferation kit, a culture-insert scratch assay, a SC aggregate sphere migration assay on the axons of dorsal root ganglions (DRGs), and a SC differentiation model. Chromatin immunoprecipitation (ChIP) united with quantitative real-time PCR (qPCR), known as ChIP-qPCR, and luciferase activity reporter assays were performed to explore the possible mechanisms by which Etv1 controls SC differentiation and myelination.

Results: The results demonstrated that Etv1 promoted myelination by facilitating SC proliferation, migration, and differentiation. Etv1 expression in SCs was upregulated during re-myelination, and knocking down Etv1 expression dramatically abrogated SC re-myelination in the crushed sciatic nerves. Moreover, silencing of Etv1 by siRNA in SCs *in vitro* inhibited its migration, proliferation, and differentiation. The results of ChIP-qPCR and luciferase reporter assay showed that Etv1 may regulate SC differentiation and myelination by binding to the promoters of myelination-related genes, such as *MAG* and *Runx2*, to initiate their transcription.

Conclusions: Taken together, these findings demonstrated a previously unknown role of Etv1 in SC differentiation and myelination, providing a candidate molecular target for clinical interventions in demyelinating diseases.

^ ORCID: 0000-0002-3124-6623.

Keywords: Etv1/Er81; Schwann cells (SCs); differentiation; myelination and re-myelination; demyelinating diseases

Submitted Jun 23, 2022. Accepted for publication Jul 29, 2022.
doi: 10.21037/atm-22-3489
View this article at: https://dx.doi.org/10.21037/atm-22-3489

Introduction

The myelin sheath of the peripheral nervous system (PNS) is formed by Schwann cells (SCs), which are multiple layers of specialized plasma membranes surrounding axons that facilitate efficient axonal signaling saltatory conduction and provide axons with the necessary nutritional support to maintain axonal integrity (1,2). Multiple peripheral nerve inherited diseases have been shown to be closely associated with dysregulated myelination, such as Charcot-Marie-Tooth disease (3,4). In addition, many extrinsic factors and pathological conditions, such as trauma, infections, or toxics, can cause myelin sheath destruction resulting in severe neurological dysfunction (5,6). Although multiple studies have been conducted to identify the genes and associated pathways that regulate myelination and regeneration (7-9), to date, the factors that facilitate the initiation of SC lineage progression (i.e., SC differentiation) and overcome barriers to successful re-myelination in demyelinating diseases are poorly defined.

Increasing evidence suggests that various intrinsic and extrinsic factors regulate the process of SC myelination. Transcriptional factors (TFs), such as early growth response 2 (Egr2, a.k.a Krox20), Sox10, and Oct6 (a.k.a. Pou3F1), are the intrinsic factors required for SCs to form and maintain myelin sheath (10). These transcriptional regulators coordinately control SC development (i.e., SC differentiation from immature to mature) and myelination. For example, Egr2, Sox10, and Oct6 activate critical myelin gene transcription by binding its promoter, or the distal and intronic enhancer sites in genes such as myelin protein zero (Mpz, also known as P0), myelin basic protein (Mbp), and peripheral myelin protein 22 (Pmp22) (11,12). In recent years, much research has focused on identifying the key regulators of myelination through various approaches, such as genomics and proteomics (13-15). We previously identified multiple potential myelination transcriptional regulators, including expressed sequence tag (ETS) variant transcription factor 1 (Etv1)/Er81, signal transducer and activator of transcription 1 (Stat1), and Sin3A, through gene microarray analysis of SCs at various stages of myelination (16).

Etv1/Er81 as a member of the ETS family that is involved in the regulation of neuronal specialization, muscle spindle differentiation, and sensorimotor connectivity (17-19). The role of Etv1 has been studied primarily in a subpopulation of spinal motor neurons, and researchers have shown that the intrinsic expression pattern and cell body localization of Etv1 coordinates motor neuron process terminal arborization (20,21). Fleming and colleagues reported that Etv1 is required in a subset of the receptor tyrosine kinase positive (RET^+) mechanosensory neurons to form the functional pacinian corpuscles, which consists of a single myelinated axon and multiple layers of non-myelinating SCs (22). Interestingly, the report also showed that Etv1 signaling pathway uses isoforms of neuregulin1 (NRG1) that are not involved in myelination in the pacinian corpuscles. Etv1 mutants were shown to cause deficient interactions between axons and corpuscle-forming non-myelinating SCs, providing evidence that neurons use different NRG1 isoforms to interact with different types of SCs. Furthermore, in the PNS, the NRG1 type III isoform has been repeatedly shown to be a key axon-derived factor that regulate SC proliferation, differentiation, and myelination by stimulating a single family of transmembrane receptor tyrosine kinases called ErbB2/3 proteins (23-25). Based on the above reports, we speculated that Etv1 may utilize the NRG1 type III isoform to promote the interaction between motor neurons and myelinating cells, thereby affecting myelination. Notably, the role of Etv1 in SC plasticity and myelin formation has so far not been described.

This current study examined the role of Etv1 in modulating myelination by affecting the biological behavior of SCs. Etv1 depletion in SCs dramatically impaired SC proliferation, migration, and differentiation, and abrogated SC re-myelination of the regenerated axons in crushed sciatic nerves. Using a combination of chromatin immunoprecipitation (ChIP) and quantitative real-time PCR (qPCR), namely ChIP-qPCR, as well as luciferase

activity reporter assay, we showed that Etv1 may initiate the transcription of myelination-related genes, such as myelin-associated glycoprotein (MAG) and Runx2, by binding to its promoter to regulate SC differentiation and myelination. These findings demonstrated a previously unknown role of Etv1 in SC differentiation and myelination, providing a candidate molecular target for clinical interventions in demyelinating diseases. We present the following article in accordance with the ARRIVE reporting checklist (available at https://atm.amegroups.com/article/view/10.21037/atm-22-3489/rc).

Methods

Screening of potential myelination-related TFs in microarray data

The transcriptomic data [Gene Expression Omnibus (GEO) Series accession number GSE163132] was obtained from our previous microarray analysis of SCs at different stages of myelination (SCs were co-cultured with neurons for 0, 1, 3, 7, 14, and 21 days). The transcriptomic data was analyzed to obtain differentially expressed genes [DEGs, $P<0.05$, fold change (FC) >1.5] using linear models and empirical bayes methods in the 'limma R' package, as previously described (26,27). The DEGs were screened and 126 TFs were obtained (Table S1). Two TF datasets (JASPAR and TRANSFAC) were then used to identify potential target genes (TRs; Table S2). The TF-TR networks were generated by using software Cytoscape 3.0.0 (28).

Animals, surgical procedures, and small interfering RNA injection

Newborn and adult Sprague-Dawley (SD) rats, as well as adult male mice were obtained from the Experimental Animal Center of Nantong University. All experimental procedures involving laboratory animals were performed under a project license (No. S20200312-003) granted by Ethics Committee of Nantong University, in compliance with the national guidelines for the care and use of animal. A protocol was prepared before the study without registration.

A total of 66 adult male mice (aged 6–8 weeks) were deeply anesthetized with 3% isofluorane before and during surgery, as previously described (29). The left sciatic nerve was exposed by incising the skin and dividing the underlying muscle. Etv1-siRNA (n=12) or control sequence (n=12) with methylation and cholesterol modifications (RiboBio, Guangzhou, China; 5 nM final concentration, 4 μL) were delivered via pressurized injection into the sciatic nerve. Three days after injection, the sciatic nerve was squeezed with a fine hemostat for 30 seconds to crush the nerve. In addition, 36 male mice were performed the sciatic nerve crush as described above, and 6 mice were used as controls (sham operated). All mice were fed and housed under routine conditions, and their conditions were monitored.

Cell culture

SCs were obtained from neonatal rats (1–2 days old) sciatic nerves. Briefly, sciatic nerves were digested with 1% collagenase (Gibco, Carlsbad, CA, USA) and 0.125% trypsin (Gibco) to obtain a cell mixture. After re-suspension and culture for 24 hours in the Dulbecco's Modified Eagle Medium (DMEM; Gibco) supplemented with 10% fetal bovine serum (FBS; Gibco), and penicillin-streptomycin (PS, Gibco), 10 mM cytosine arabinoside (Sigma, St Louis, MO, USA) were added in culture medium to remove the fibroblasts. After treatment for 24 hours, the medium was changed with DMEM supplemented with 10% FBS, 5 μM forskolin (Sigma), 2 ng/mL neuregulin 1 (NRG1; R&D, MN, USA), L-glutamine (Gibco), and PS, to stimulate SC proliferation. SCs were purified with anti-Thy1 antibody (1:1,000, Sigma) to remove any residual contaminating fibroblasts when cell growth and covered 90% of the culture dish. The purity of the SCs was assessed by the SC marker S100β (1:500, Sigma) immunofluorescence staining.

The dorsal root ganglion (DRG) neurons were obtained from embryonic day (E) 15 rats, as previously described (30). After digesting with 1% collagenase and 0.125% trypsin for 30 minutes at 37 ℃, the DRG cells were rinsed and mechanically dissociated with DMEM medium supplemented with 5% newborn bovine serum. Following purification by a differential velocity adherent technique, the culture medium were changed with the serum-free neurobasal medium (Gibco) supplemented with 50 ng/mL nerve growth factor (Sigma), 2 mM L-glutamine (Gibco) 2% B27 (Gibco). Furthermore, the neurons were obtained by depleting non-neuronal cells with neural basal (NB) medium containing 5-fluorodeoxyuridine (Sigma) and uridine (Sigma) during culture. The DRG neuron purity was assessed by β-III tubulin (TuJ1, 1:500, Abcam, Cambridge, England) immunofluorescence staining.

All cell culture plates, dishes, and coverslips were coated with 50 μg/mL poly-L-lysine (PLL; Sigma) for at least

30 min at room temperature (RT), then rinsed 3 times in distilled water and sterilized in a clean bench.

SC differentiation assay

SCs with a density of approximately 1×10^4 total cells per 500 µL were plated onto PLL-coated 24-well plates, and induced their differentiation as previously described (16). In brief, SCs were first incubated with DMEM supplemented with 10% FBS for 24 hours, thereafter, the medium were changed with DMEM containing 20 ng/mL human recombinant NRG1 (HRG, R&D), 1 mM dibutyryl cyclic adenosine monophosphate (db-cAMP; Sigma), and 1% FBS. SCs were cultured for 3 days to induce their differentiation, and then differentiated cells were subjected to Western blotting (WB) and immunocytochemistry (ICC) to analyze MAG and P0 expression.

SC migration assays

The migration ability of SCs was assessed using the following two methods: (I) the scratch assay based on a culture-insert (Ibidi, DE, Germany); and (II) the SC aggregate sphere migration assay as described previously (31). For the scratch assay, 5×10^3 SCs were seeded in 80 µL of medium onto ibidi inserts which were placed into 24-well plates. After cultivation for approximately 24 hours, the culture-inserts were removed to create a cell-free gap where the situation of cell migration could be observed. In the migration medium, which contains 2 µg/mL mitomycin C (Sigma) to inhibit cell proliferation, cells on both sides of the scratch were incubated for 12 hours at 37 ℃, and then the Image J software (NIH Image J 1.46R) was used to measure the width of the scratch. Furthermore, the SC aggregate spheres migration assay was used to observe the effect of Etv1 on the migration of SCs growing on axonal membranes. Briefly, SC aggregated spheres were obtained by culturing SCs overnight on a substrate that did not allow their adherence, with gentle shaking several times every 2–3 h. The fasciculated DRG axonal membrane was achieved by plating DRG neurons onto one side of a PLL for 2–3 weeks. After culturing the SC aggregated spheres on a fascicular axon membrane or PLL-coated coverslip for 12 hours, they were observed and photographed with a microscope (Leica, Bensheim, Germany), and NIH Image J 1.46R software was used to measure the area of SC migration.

SC proliferation experiment

The EdU DNA Cell Proliferation Kit (RiboBio) was used to observe the effect of Etv1 on SC proliferation. Briefly, approximately 4×10^4 SCs were plated onto 24-well plates coated with fascicular axons or PLL, and incubated in DMEM containing 50 µM EdU and 10% FBS for 24 hours. Cells were then fixed with 4% paraformaldehyde at RT for 30 minutes, followed by three washes with phosphate buffered saline (PBS), EdU antibody (1:1,000) were added and incubated with cells for 2 hours at RT, and Hoechst 33342 (1 µg/mL, Sigma) were used to label the cell nuclei with following two washes with PBS. Ten random fields were selected from each well and photographed with a fluorescence microscope (Leica). Experiment was repeated at least three times, and three wells were visualized for each experiment to determine the EdU positive cell percentage out of total cells.

RNA interference assay

RiboBio synthesized and purified short interfering RNA (siRNA) oligonucleotides targeting Etv1 (Etv1-siRNA) were used in this study and their sequences are provided in Table S3. After seeding purified SCs at a density of 3×10^6 cells/mL and incubating in 24-well plates for 24 hours, SCs were transfected with 10 nM Etv1-siRNA and a non-targeting negative control (scramble) by using transfection reagent Lipofectamine RNAiMAX (Invitrogen, Carlsbad, CA, USA) according to the instructions of manufacturer. Thereafter, cells were lyzed in Trizol (Invitrogen) or protein lysis buffer buffer (RIPA; Pierce, Rockford, IL, USA) 48 hours post transfection to extract total RNA or total protein for real-time reverse transcription polymerase chain reaction analysis (RT-qPCR) and WB analysis, respectively.

RNA isolation and RT-qPCR

RNeasy Plus Mini kit (Qiagen, Valencia, USA) was used to extract total RNA from cultured cells, and complementary DNAs (cDNAs) were synthesized with the Reverse Superscript Kit (Invitrogen) following the manufacturer's instructions. RT-qPCR was conducted using SYBR green Premix (Life Technologies, Gaithersburg, MD, USA) on a StepOnePlus Real-Time PCR System (ABI, Foster, CA, USA). Three replicates were set for each experiment, and three independent experiments were repeated. The ΔΔCT

method was used to calculate the relative expression levels of the control groups and the experimental groups, and glyceraldehyde 3-phosphate dehydrogenase (GAPDH) was used to normalize the original data. The sequences of primer can be found in Table S4.

Western blotting analysis

The lysis buffer (Pierce) containing 2% sodium dodecyl sulfate (SDS), 10 mM ethylene diamine tetra acetic acid (EDTA), 95 mM NaCl, 25 mM Tris-HCl (pH 7.4), as well as protease and phosphatase inhibitors, was used to prepare nerve and cell protein lysates. After being sonicated, the protein lysates were centrifuged at 13,200 rpm for 15 minutes at 4 ℃, and the protein concentration was quantified with BCA protein quantification kit (Beyotime, Shanghai, China). Twenty micrograms of proteins were separated using a 10–15% SDS-polyacrylamide gel and blotted onto polyvinylidene fluoride (PVDF) membranes purchased from Millipore (Millipore, MA, USA). After being blocked with 5% skim milk containing 0.1% Tween-20 at RT for 1 hour, the membranes were probed overnight at 4 ℃ with the primary antibodies, as follows: Etv1 (PA5-41484, Invitrogen, 1:200), MAG (34-6200, Invitrogen, 1:100), and GAPDH (60004-1-Ig, Proteintech, 1:20,000, Chicago, USA). Thereafter, the membranes were washed with Tris buffered normal saline (TBS) 3 times, and then incubated with the corresponding secondary antibodies (1:1,000) conjugated with horse radish peroxidase (HRP) at RT for 1 hour. After reacting with the SuperSignal West Pico Chemiluminescent Substrate Kit (Pierce), the protein signals were detected with a densitometer scanner (GS800, Bio-Rad, Richmond, CA, USA).

ICC and immunohistochemistry (IHC)

After being fixed in 4% paraformaldehyde (PFA) for 30 minutes at RT and three washes with PBS, cells were permeabilized for 30 minutes with PBS containing 0.1% Triton X-100, and then blocked for 1 hour at RT with 5% normal donkey serum. Cells were then incubated with appropriately diluted primary antibodies overnight at 4 ℃ and the corresponding secondary antibodies conjugated by fluorescence for 1 hour at RT, with several washes in between. After being counterstained with Hoechst 33342 (Sigma), the cell images were captured with a fluorescence microscope purchased from Carl Zeiss Microscopy (Thornwood, NY, USA).

After being post-fixed in 4% PFA and dehydrated in 20% sucrose, the nerve tissues were embedded into optimal cutting temperature compound (OCT). The 12 μm thick tissue sections cut by a cryostat were used to perform IHC. After blocking with 10% donkey serum in PBS-Tween (PBS-T) for 2 hours at RT, the sections were reacted with primary antibodies and corresponding secondary antibodies in the same process as ICC. The images were acquired with a Zeiss Observer fluorescence microscope. At least 3 animal samples were taken for analysis in each group, and the experiment was repeated for 3 times.

The following primary antibodies were used: S100β (S2532, Sigma, 1:200), MAG (34-6200, Invitrogen, 1:100), β-III tubulin (TuJ1, MMS-435P, Covance, Berkeley, USA, 1:200), Etv1 (PA5-41484, Invitrogen, 1:200); The secondary antibodies (1:1,000; Jackson Immuno Research, West Grove, PA, USA) as follows: Alexa Fluor® 488 donkey anti-mouse (715-545-151) and anti-rabbit (711-545-152), Cy™3 donkey anti-mouse (715-165-151) and anti-rabbit (711-165-152).

Transmission electron microscopy (TEM)

For myelin sheath ultrastructural analysis, sciatic nerves were fixed with 2.5% glutaraldehyde which diluted in 0.1 M phosphate buffer (pH 7.2) and post-fixed with 1% osmium tetroxide. After being dehydrating, nerves were embedded into Epon 812 epoxy resin and cut into 50 nm thick ultra-thin sections, which were then stained with lead citrate and uranyl acetate. A transmission electron microscope (JEOL Ltd., Tokyo, Japan) was used to observe the stained specimens. With at least 3 animals per group, images were captured from at least 10 randomly selected fields per animal to determine the *g*-ratio, myelin sheath thickness, axon diameter, as well as the number of myelin sheath layers.

ChIP-qPCR

The database of eukaryotic promoter (http://epd.vitalit.ch/) was used to choose the promoter regions of Etv1 binding and repression. The gene promoter region in this study was use the rat genome version rn6 as follows: MAG [positions 89,360,666-89,363,285 on chromosome (Chr) 1], P0 (positions 89,521,180-89,524,289 on Chr 13), Pmp22 (positions 49,535,934-49,538,691 on Chr 10), Zeb2 (positions 29,984,109 and 29,987,005 on Chr 3), and Runx2 (positions 18,562,029-18,564,997 on Chr 9), was divided

into 2–3 parts for the design of primers, and each part was designed with a pair of primers. Primer sequences are provided in Table S5.

After fixation with 1% formaldehyde (Life Science, Louis, MO, USA) for 20 minutes, the pooled differentiating SCs were lysed and sonicated using a cell crusher (Scientz, Shanghai, China) at 29% power with 1 second interval on and off for 9 minutes until the DNA was fragmented to between 200 and 1,000 bp in lengths. The sheared chromatin was incubated with 5 μg of Etv1 antibody (Invitrogen, PA5-77975) at 4 ℃, and the Magna ChIP G Kit (Millipore) was used to perform the ChIP assay in accordance with the manufacturer's guidelines. Using SYBR green PCR mix (Life Technologies), RT-qPCR and the $2^{-\Delta CT}$ method were used to determine the relative fold enrichments of normalized samples to input chromatin.

Luciferase reporter assay

DNA fragments corresponding to promoters of these genes (the region is same as mentioned in the ChIP-qPCR), including wild-type and mutant types, were obtained by PCR and subcloned into the pGV238 luciferase expression vector (Genechem, Shanghai, China) between KpnI and XhoI sites. DNA sequencing was performed to confirm these constructs. The primer sequences can be found in Table S6.

The human embryonic kidney cell line (HEK293) was cultured with DMEM supplement with 10% FBS for 24 hours, and then cotransfected with the luciferase plasmids carrying the promoter sequence and a pGV141-Etv1 (NM_001163156) expression vector containing the Renilla luciferase gene using the Roche X-tremegene HP DNA Transfection Reagent. After a 48-hour transfection, the luciferase activity was measured with the Dual-Luciferase Assay System (Promega), examining the ratio of firefly luciferase activity to Renilla luciferase activity and normalized to the ratio of the pGV238 base vector.

Quantification and statistical analysis

Data are expressed as mean ± standard deviation (SD) unless otherwise indicated. One-way analysis of variance (ANOVA) was used for comparisons between three or more groups, while unpaired two-tailed *t*-tests were used for comparisons between two groups. The P values are indicated by asterisks as follows: *P<0.05, **P<0.01, and ***P<0.001. The experiment was kept double-blind, that is, animal grouping, reagent injection, animal surgery, result evaluation and data analysis were performed by different experimenters. The processing software for data analysis included Microsoft Excel (Microsoft Office, DC, USA), Microsoft PowerPoint (Microsoft Office), GraphPad Prism 8.0 (GraphPad Software, CA, USA), and Image J (NIH, MD, USA).

Results

Identification of potential TFs by analyzing the transcriptomic data of myelinating SCs

The transcriptomic data (GSE163132) obtained from our previous microarray analysis of SCs at different stages of myelination (SCs co-cultured with neurons for 0, 1, 3, 7, 14, and 21 days) was analyzed to identify the differentially expressed genes (DEGs, P<0.05, FC >1.5) using the 'R' software package, as previously described (26,27). Among these DEGs, there were the 126 TFs (Table S1). Based on the FC in gene expression compared to the control (day 0), the top 20 TFs were selected to construct a heat map (*Figure 1A*). Etv1 showed the highest FC, and its expression trend increased from day 1, peaked on day 7, and then gradually decreased, and this was similar to other TFs related to myelination such as Egr2, Pou3f2, and myelin gene regulatory factor (Myrf). In addition, the qRT-PCR results further confirmed that Etv1 and these three TFs (Egr2, Pou3f2, and Myrf) have similar expression trajectories (*Figure 1B*). The above data suggested that Etv1 may participate in myelination.

Given that TFs must bind to the promoters or enhancers of their target genes to exert their regulatory roles, a TF-binding site enrichment analysis was performed for Etv1 and other 3 myelination-related TFs, including Egr2, Sin3A, and Zeb1 (based on two TF datasets, JASPAR and TRANSFAC). The predicted TRs was intersected with the DEGs from the transcriptome data to avoid confounders and identify the most statistically robust differential TRs (Table S2). The TF-TR network was constructed using the Cytoscape software (*Figure 1C*). Interestingly, Etv1, Egr2, Sin3A, and Zeb1 occupied relatively distinct network territories and targeted different TRs, suggesting that the four TFs regulated SC myelination by controlling distinct gene sets (*Figure 1C*). Remarkably, the four TFs shared eight TRs, including Prkca, Sqstm, Gdap1, Smad7, Clcn2, Nab2, Lmnb1, and Srebf1, suggesting that they regulated myelination not completely independently, but in a coordinated and orderly manner.

Therefore, Etv1 may be involved in the regulation of

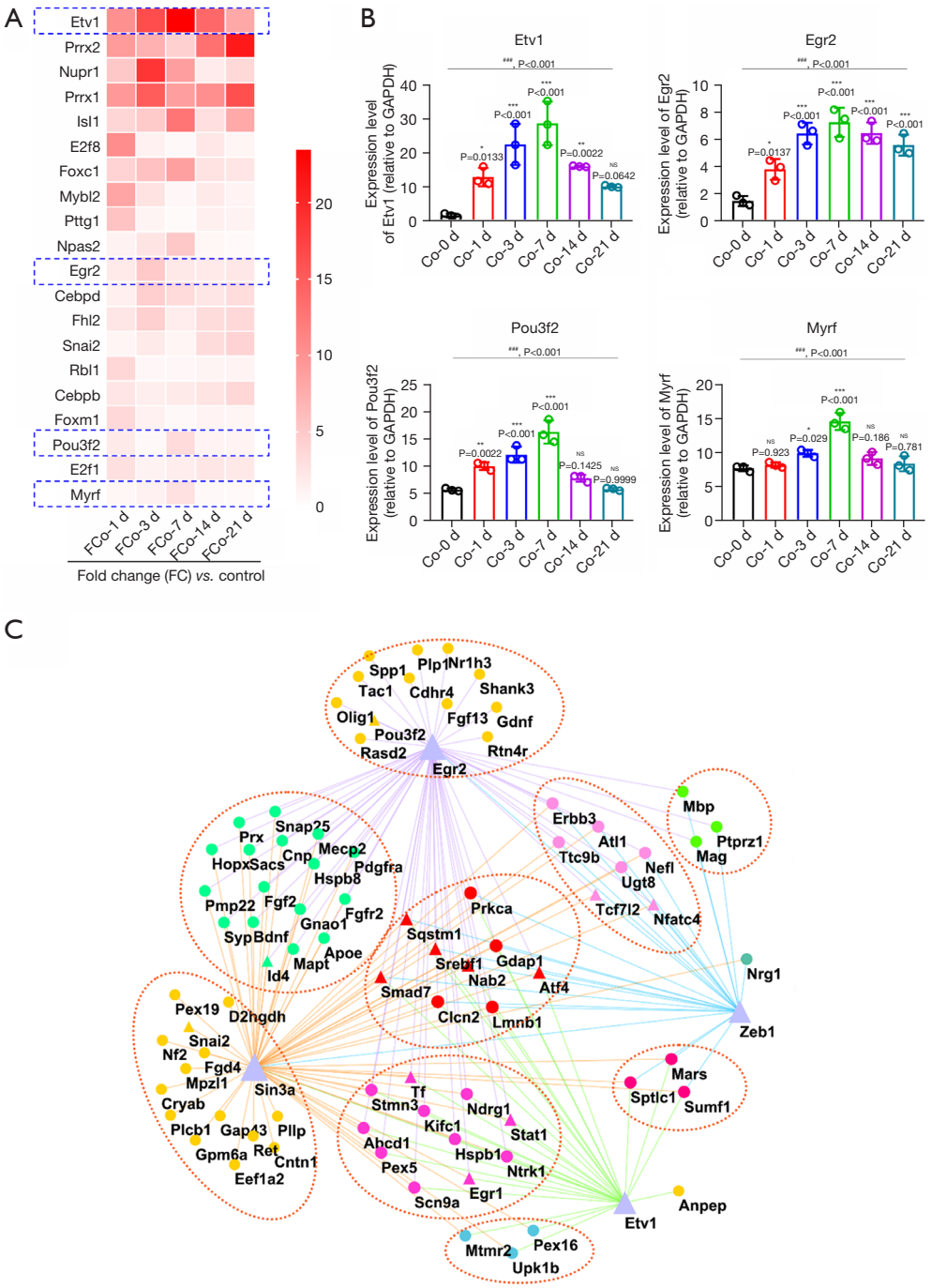

Figure 1 Screening for myelination-related TFs by analyzing the transcriptomic data of myelinating SCs. (A) The heatmap shows the top 20 signature TFs (rows) with FCs >2 compared to day 0 during SC myelination (columns: FC versus co-0 d). The blue dotted box indicates the genes, including Etv1, Egr2, Pou3f2, and Myrf, with the same expression trend. (B) qPCR showing the gene expression of Etv1, Egr2, Pou3f2, and Myrf in SCs during myelination. ###, P<0.001, one-way ANOVA; *, P<0.05, **, P<0.01, ***, P<0.001 *vs.* co-0 d, n=3 per group. (C) The regulatory network of the TFs. Nodes correspond to genes, triangles correspond to TFs, and dashed circles correspond to interactions. The over-represented TFs (triangles) are shown in purple, such as Etv1, Egr2, Sin3a, and Zeb1. The triangle size is based on its centrality. NS, no statistical difference; GAPDH, glyceraldehyde 3-phosphate dehydrogenase; TF, transcription factor; SC, Schwann cell; FC, fold change; qPCR, quantitative polymerase chain reaction; ANOVA, analysis of variance.

myelination, similar to Egr2, Sin3A, and Zeb1. *In vitro* and *in vivo* experiments were conducted to further examine the effects of Etv1 on myelination.

Etv1 expression and cellular location following sciatic nerve crush

An *in vivo* mouse myelination model, involving crushing of the sciatic nerve, was used to investigate the potential role of Etv1 in controlling myelination. WB analysis was used to assess the MAG and Etv1 protein expression in the sciatic nerves on days 1, 4, 7, 14, 21, and 28 after crushing of the nerve (*Figure 2A*). The expression of Etv1 decreased drastically at day 1 after nerve injury and then gradually up to day 28. In contrast, MAG expression decline from day 1, reached a minimum at day 4, and then increased again reaching a peak on day 28, consisting with the destruction and clearance of myelin sheath in the early stages of nerve injury (days 1 and 4) and re-myelination in the later stages of injury (days 7–28). These data suggested that Etv1 may be involved in the regulation of myelination during nerve regeneration. Double immunofluorescence staining with Etv1 and S100β (an SC marker) was performed to observe the cellular localization of Etv1 in the crushed site of the injured sciatic nerve. The entire colocalization of Etv1 and S100β was not observed until 7 days after injury, whereas only a small amount of SCs expressed Etv1 at 1 and 4 days after injury (*Figure 2B*), suggesting that Etv1 located in SCs may participate in re-myelination initiated 7 days after nerve crush.

Etv1 knockdown inhibits re-myelination of regenerating axons

To determine the role of Etv1 on SC re-myelination after nerve injury, 3 siRNAs against Etv1 (Etv1-siRNAs) were synthesized and transfected into SCs. The efficiency of knockdown was assessed by WB analysis. The Etv1-siRNAs all resulted in an approximately 4-fold reduction in Etv1 levels compared to the scrambled siRNAs (Figure S1). Given the higher transfection efficiency and longer duration of action of cholesterol-modified siRNA (32,33), an orthotopic injection of cholesterol-modified Etv1-siRNA into the sciatic nerve was used to knock down the expression of Etv1, and the effect was assessed 3 days following infection. The expression level of Etv1 in the Etv1-siRNA interference group was lower compared to the control group, suggesting that cholesterol-modified siRNA could effectively knock down the protein expression of Etv1 in the sciatic nerve (*Figure 3A*).

Sciatic nerve crush injury was performed in mice 3 days after in-situ injection of Etv1-siRNA, and the expression of MAG in the injured sciatic nerve was evaluated by WB (*Figure 3B*.b1) and IHC (*Figure 3B*.b2) on day 28 after the injury. The results showed that the level of MAG was lower in Etv1 knockdown mice than in controls. Furthermore, the results of TEM showed that the myelin sheaths of the control mice had the perfect SC basal membrane and the lamella densely surrounded the regenerated axons, while in the Etv1-siRNA treated groups, SC myelination was abnormal, manifesting as hypermyelination or hypomyelination. Quantitative analysis showed that the ratio of myelinated/unmyelinated axons, the myelin sheath layer number, and the myelin sheath thickness were all lower, while g-ratio, a reliable axonal myelination index (34), was higher in the Etv1 knockdown mice than in the control (*Figure 3B*.b3). Together, these observations suggested that Etv1 regulates SC re-myelination *in vivo*.

Knockdown of Etv1 in SCs reduces proliferation in vitro

Etv1 effects on SC proliferation was evaluated with the Edu labeling kit (*Figure 4*). SCs treated with Etv1-siRNA or a non-targeting negative control (scrambled siRNA) were cultured on PLL or fasciculated axon member of DRG neurons, and the proliferation rate was estimated. In both isolated (*Figure 4A*) and co-cultured SCs (*Figure 4B*), the number of EdU and Hoechst double-labeled cells in SCs treated with Etv1-siRNA was significantly lower than that in cells treated with the scrambled siRNA, suggesting that SC endogenous ETV1 can positively regulate the its proliferation regardless of external conditions such as DRG neurons.

Knockdown of Etv1 in SCs decreases migration in vitro

To explore whether Etv1 affects SC migration, insertion-based scratch migration assays were performed after transfection of SCs with Etv1-siRNA or a scramble, and the cell migration area analysis was performed 12 hours after removal of the insert. The results showed that SCs transfected with Etv1-siRNA migrated approximately three-fold less than the negative control (*Figure 5A*), indicating that Etv1 knockdown prevented SC migration. Given that axonal signaling affects SC behavior under physiological conditions, an alternative migration assay

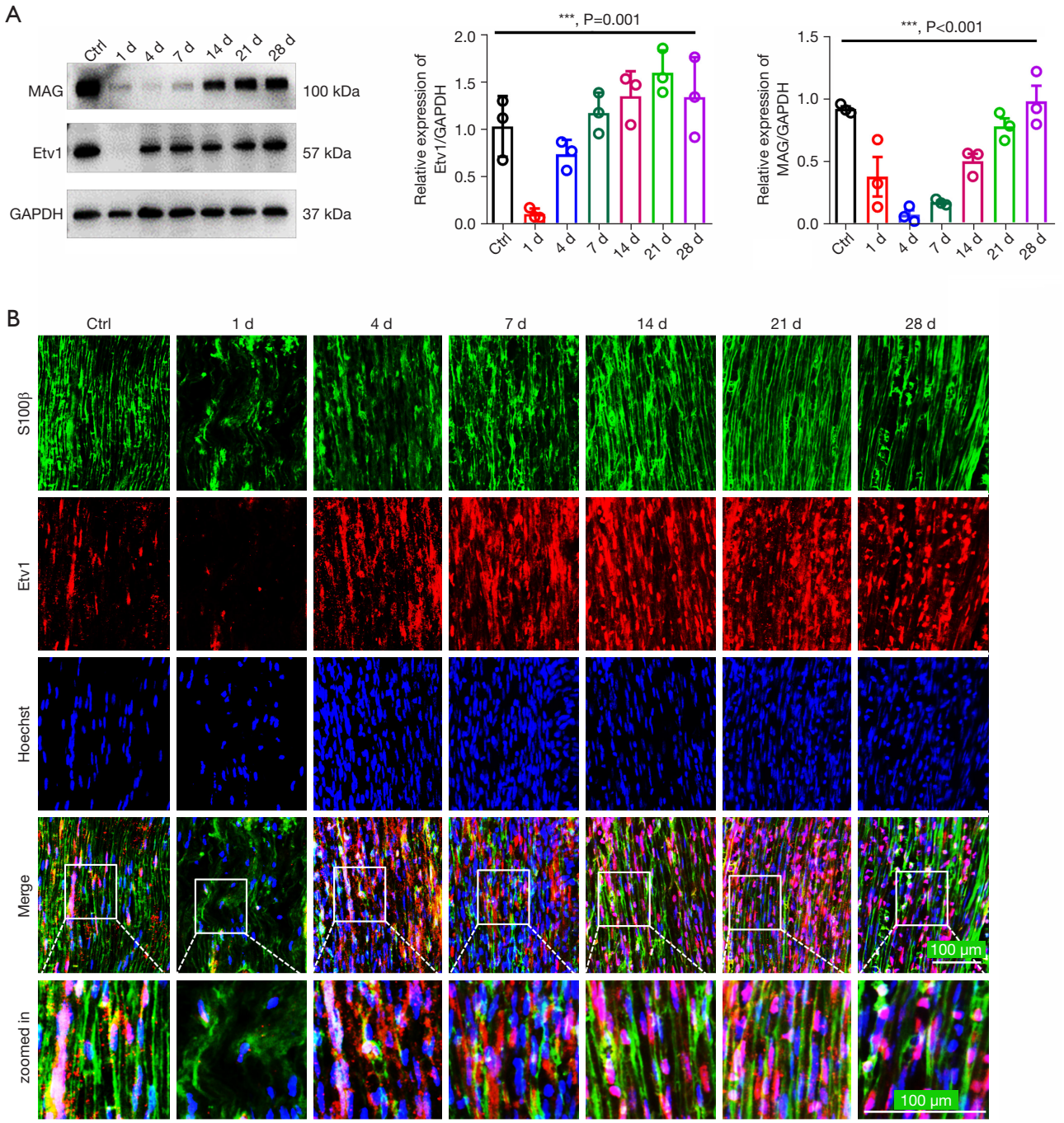

Figure 2 Etv1 expression and cellular localization in the crushed mouse sciatic nerve. (A) WB analysis showing the expression of Etv1 and MAG in nerves on days 1, 4, 7, 14, 21, and 28 after nerve injury. The uninjured nerve served as the control (Ctrl). Quantitative statistical comparisons of Etv1 and MAG protein levels in regenerated nerve segments after nerve crush are shown in the histograms. ***, P<0.001, one-way ANOVA, n=3 per group. (B) Immunofluorescence staining of the injured sciatic nerve sections of mice show only a small amount of Etv1 and S100β co-localization on day 1 post-injury. Etv1 is mainly localized in SCs from day 4 after injury. Scale bar =100 μm. S100β (a marker of SCs) is stained green and Etv1 is stained red. MAG, myelin-associated glycoprotein; GAPDH, glyceraldehyde 3-phosphate dehydrogenase; SC, Schwann cell; WB, Western blotting; ANOVA, analysis of variance.

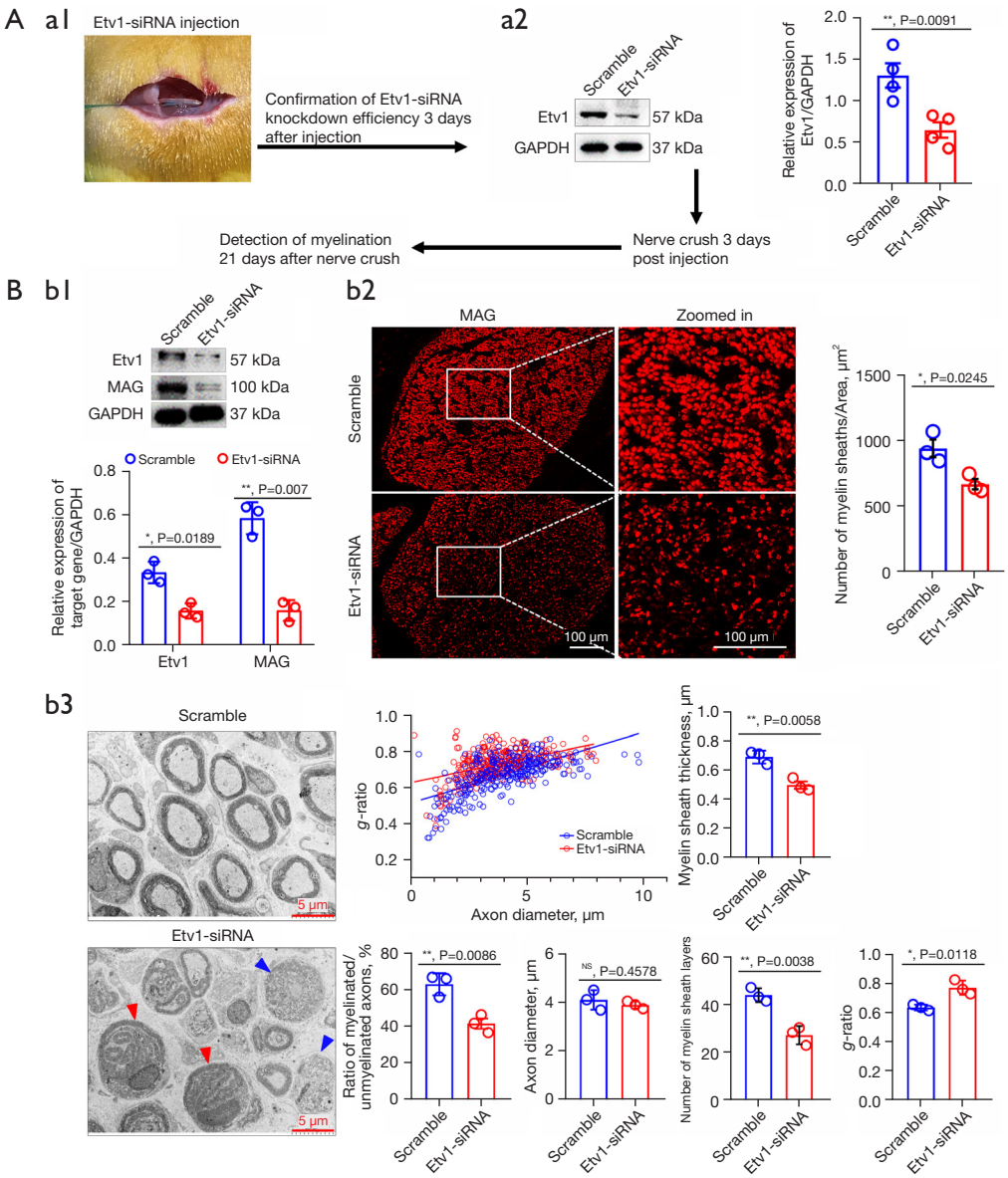

Figure 3 Etv1 knockdown inhibits remyelination after sciatic nerve crush. (A) The schematic diagram showing the experimental process. (a1) A representative diagram of the Etv1-siRNA injection into the mouse sciatic nerve. (a2) WB showing the knockdown efficiency of the Etv1-siRNA on day 21 post virus injection. The histogram shows the changes in protein levels of Etv1 in the nerve. **, P<0.01 *vs.* control (scramble); *t*-test; n=3 per group. (B) Etv1 knockdown inhibits remyelination after sciatic nerve crush. (b1) WB shows MAG and Etv1 levels in the nerves transfected with Etv1-siRNA at 21 days after nerve injury. GAPDH was used as the internal standard. *, P<0.05, **, P<0.01 *vs.* scramble; *t*-test; n=3 per group. (b2) MAG immunostaining (red) shows SC re-myelination in Etv1-siRNA and scramble treated nerves. Scale bar =100 μm. Quantitative statistical comparison of the myelin sheath density is shown in the histograms. *, P<0.05 *vs.* scramble, *t*-test, n=3 per group. (b3) The transmission electron micrographs showing the myelin sheaths of the regenerated nerve treated with Etv1-siRNA and scramble at 21 days after surgery. Red arrow head, hypermyelination; blue arrow head, degenerated myelin sheath. Scale bars =5 μm. The *g*-ratio, axon diameter, myelin sheath layer number, thickness, and the ratio of myelinated/unmyelinated axons, were compared between Etv1-siRNA and scramble treated groups. *, P<0.05; **, P<0.01 *vs.* scramble; NS, not significant; *t*-test; n=3 per group. siRNA, small interfering RNA; WB, Western blotting; GAPDH, glyceraldehyde 3-phosphate dehydrogenase; MAG, myelin-associated glycoprotein; SC, Schwann cell.

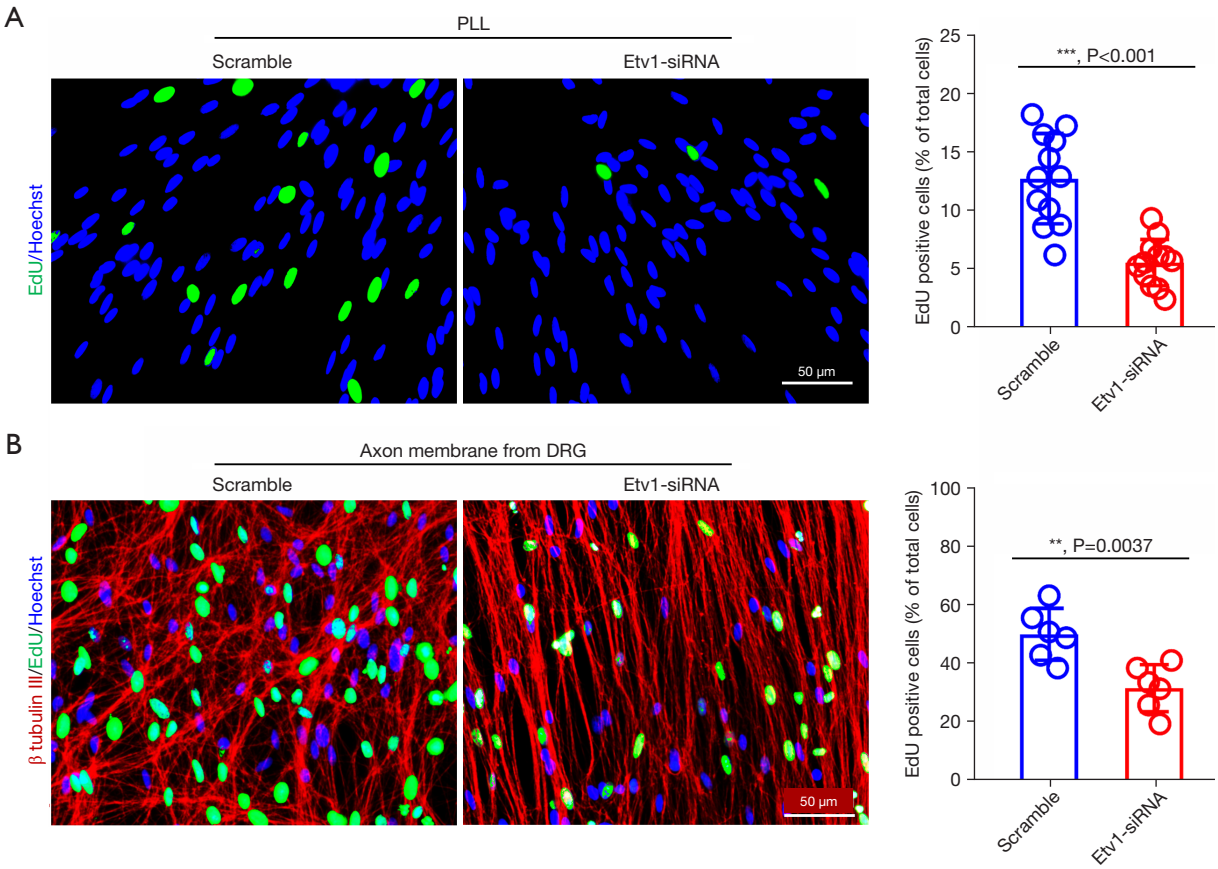

Figure 4 Etv1 knockdown reduces the proliferation of SCs. (A) The proliferation of SCs seeded on PLL transfected with Etv1-siRNA or scramble-transfected was detected using EdU labeling kits. Proliferating SCs are stained with EdU (green) and Hoechst (blue) is used to mark cell nuclei. Scale bar =50 μm. The histogram shows that knockdown Etv1 in SCs cultured on PLL significantly decreased their proliferation. ***, P<0.001 *vs.* scramble; *t*-test; n=12. (B) Proliferation ratio of SCs transfected with Etv1-siRNA or scramble seeded on fasciculated DRG axons. Proliferating SCs are stained with EdU (green), fasciculated DRG axons are stained with β tubulin III (red), and Hoechst (blue) is used to mark cell nuclei. Scale bar =50 μm. Histograms showing that knockdown Etv1 in SCs cultured on fasciculated DRG axons significantly reduced their proliferation **, P<0.01 *vs.* scramble; *t*-test; n=6. PLL, poly-L-lysine; siRNA, small interfering RNA; DRG, dorsal root ganglion; SC, Schwann cell.

was conducted as previously reported (29,31). Briefly, SCs were seeded as spheroids on the bundled axons of DRG neurons, and the distance that cells migrated out of the spheroid after 12 hours of cultivation was assessed. The results showed that Etv1-siRNA-transfected SCs growing on fascicular DRG axons migrated significantly slower from the reaggregates compared to control cells, which was similar to the results obtained in the scratch migration assay above (*Figure 5B*). These observations suggested that endogenous Etv1 can positively regulate the SC migration regardless of external conditions such as DRG neurons.

Knockdown of Etv1 in SCs antagonizes their differentiation in vitro

An *in vitro* SC differentiation assay as previously described (35,36) combined with RNA interference technology, was used to investigate the effect of Etv1 on SC differentiation. After 3 days of treatment with 1 mM dB-cAMP and 20 ng/mL HRG, SCs became flattened, and ICC and WB results showed SCs had high expression of MAG, a marker representing mature or myelinating SCs. This indicating that the SC differentiation model was successfully established (*Figure 6A*). Furthermore, the expression of Etv1 increased during SC differentiation (*Figure 6B*.b1). Next,

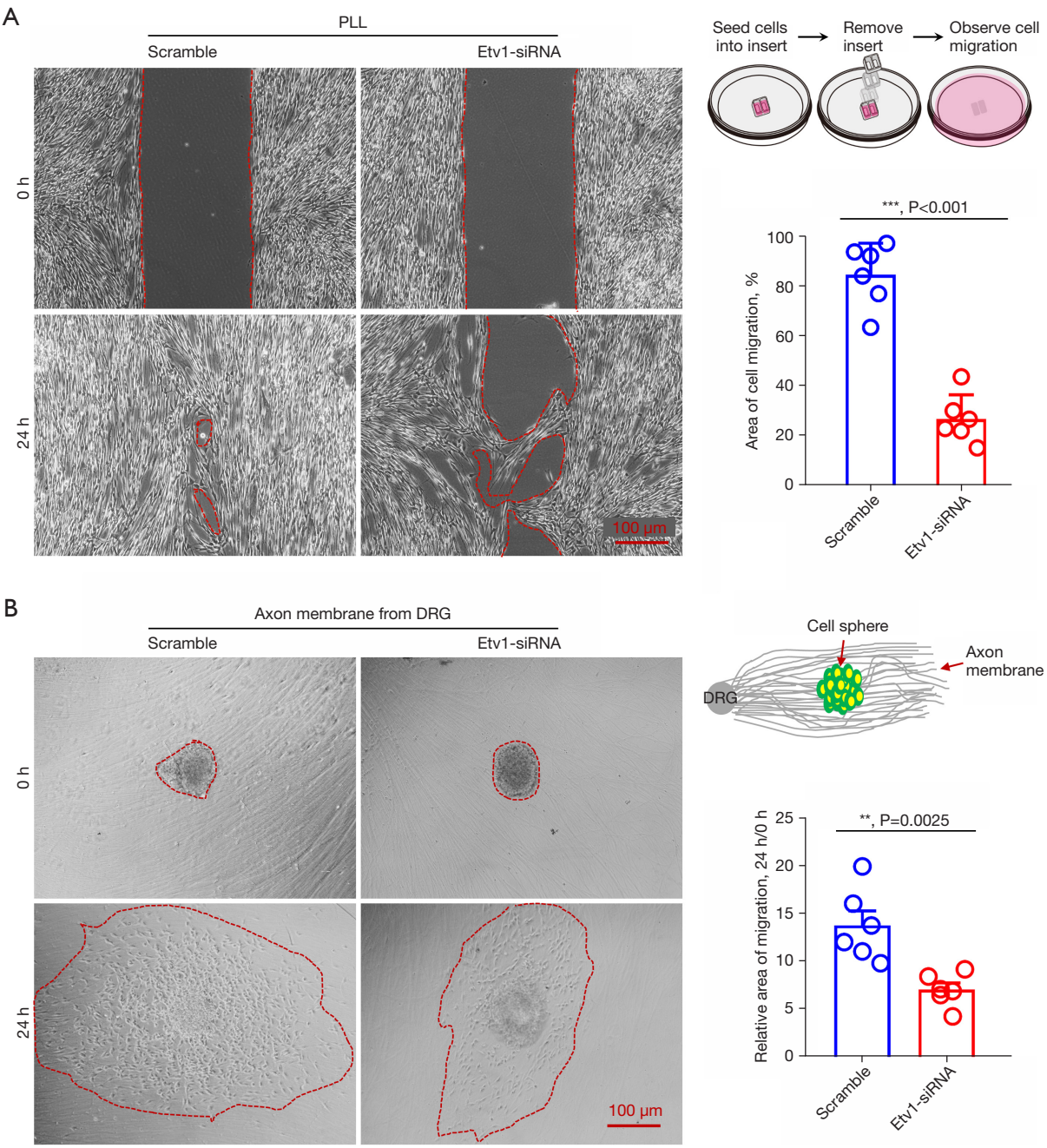

Figure 5 Knockdown of Etv1 in Schwann cells inhibits its migration ability. (A) The insert-based scratch migration assay. The histogram shows that Etv1 knockdown in SCs decreased its migration ability compared to SCs transfected with the scrambled vector. ***, P<0.001 *vs.* scramble; *t*-test; n=6. Representative phase contrast microscopy images (left) were selected from 6 independent experiments. Scale bar =100 μm. The schematic diagram showing the experimental procedure (top right). (B) The phase contrast microscopy images show that the SCs reaggregate on fasciculated DRG axons following treatment with Etv1-siRNA and scramble. The area inside the red dashed line represents the distance of SC migration. Scale bar =100 μm. The schematic diagram on the top right showing the experimental procedure. The histogram shows that Etv1 knockdown in SCs growing on fascicular DRG axons inhibits their migration out of the reaggregated SC spheres. **, P<0.01 *vs.* scramble; *t*-test; n=5. PLL, poly-L-lysine; siRNA small interfering RNA; DRG, dorsal root ganglion; SC, Schwann cell.

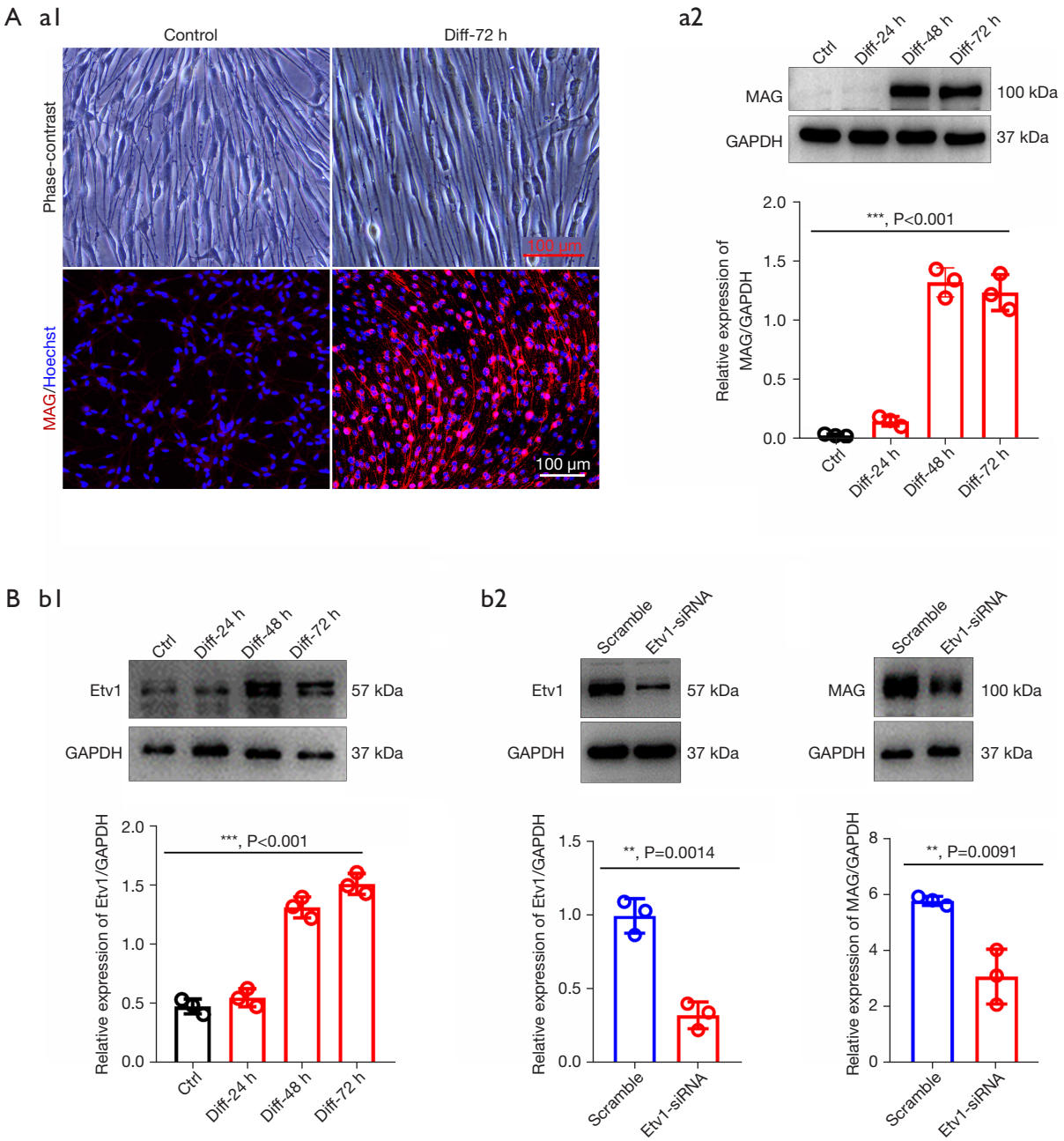

Figure 6 Etv1 knockdown in Schwann cells antagonizes its differentiation. (A) (a1) Representative images of phase contrast microscopy and ICC analysis, showing that dB-cAMP can effectively induce SC differentiation. Red staining represents MAG expression and cell nuclei (blue) are marked with Hoechst staining. Scale bar =100 μm. (a2) WB comparing the expression of MAG in SCs treated with dB-cAMP or vehicle for 24, 48, and 72 hours. ***, P<0.001; one-way ANOVA; n=3 per group. (B) (b1) Western blot comparing Etv1 levels in SCs differentiated for 24, 48, and 72 hours. ***, P<0.001; one-way ANOVA; n=3 per group. (b2) WB showing Etv1 and MAG expression in differentiated SCs transfected with Etv1-siRNA and scrambled siRNA. The histogram shows that the knockdown of Etv1 in SCs significantly reduced the expression of MAG after the induction of differentiation. Student's *t*-test; **, P<0.01 *vs.* scramble; n=3 per group. MAG, myelin-associated glycoprotein; GAPDH, glyceraldehyde 3-phosphate dehydrogenase; Ctrl, control; Dif, differentiation; siRNA, small interfering RNA; ICC, immunocytochemistry; SC, Schwann cell; WB, Western blotting; ANOVA, analysis of variance.

differentiation was induced in SCs transfected with Etv1-siRNA or scrambled siRNA. After 3 days, the differentiation of Etv1-siRNA transfected SCs was significantly blocked, as shown by the significantly lower levels of MAG expression than in scrambled siRNA transfected cells (*Figure 6B*.b2). These results suggested that Etv1 could promote SC differentiation in an *in vitro* differentiation model.

Etv1 may recruit myelination-related genes to regulate SC differentiation

Given that SC differentiation is the most critical step for myelination (8), the differentiating SCs were used to investigate the potential mechanisms by which Etv1 regulates SC myelination. ChIP experiments were performed using pooled differentiating SCs. The qPCR results revealed that Etv1 enriched the amplified fragments from P0, Pmp22, Runx2, and MAG promoters, but failed to recruit Zeb2, although its fragments contained typical Etv1 binding sites, compared to the control, namely, ChIP experiments treated with IgG without Etv1 antibody (*Figure 7A*). These results suggested that Etv1 may bind with the promoters of these four genes (P0, Pmp22, Runx2, and MAG) to play a regulatory role in differentiated SCs. Luciferase gene reporter assays using HEK293 cells were conducted to further confirm the interaction of Etv1 and the four target genes, and results showed co-transfection of Etv1 and the Runx2 promoter, as well as Etv1 and the MAG promoter, into cells resulted in a significant upregulation of luciferase activity compared to control cells. In contrast, co-transfection of Etv1 and the other 2 promoters, P0 and Pmp22, had little effect on luciferase activity (*Figure 7B*). These data suggested that Etv1 may initiate the transcription of MAG and Runx2 by binding to the promoter region to regulate SC differentiation and myelination (*Figure 7C*).

Discussion

This study identified a previously unknown role of Etv1 in SC differentiation and myelination. In contrast with other ETS domain TF superfamily members, Etv1 has been implicated in controlling the formation of functional connections between sensory afferents and motor neurons (17), the terminal maturation program of cerebellar granule cells (18), and the establishment of motor innervation of adjacent muscles (21). Based on the data analysis of gene expression profiles of myelinating SCs (*Figure 1* and Table S1) and the *in vitro* and *in vivo* experiments, our study demonstrated that Etv1 depletion in SCs dramatically impairs SC proliferation, migration, and differentiation, and abrogates SC re-myelination in the regenerated sciatic nerves. Furthermore, this report showed that Etv1 may regulate myelination through binding the promoters of myelination-related genes, such as MAG and Runx2, to initiate their transcription.

To identify the potential role of Etv1 in myelination and re-myelination, its expression and cellular localization in PNS tissues (such as the DRG and sciatic nerve) and PNS cells (such as SCs and DRG neurons), were examined. IHC revealed that Etv1 was expressed and localized in the nucleus of SCs in sciatic nerve tissue and cultured SCs, as well as DRG neurons, mainly in the nucleus (Figure S2A). Since the Etv1 gene is highly expressed in sciatic nerves and SCs compared to neurons (Figure S2B), further investigations were conducted using SCs. Experiments with the *in vivo* myelination model demonstrated that Etv1 and MAG similarly increased from day 7 post-nerve injury. However, the expression patterns differed in the early stages of nerve injury (1–4 days), with Etv1 expression decreasing sharply on the first day after nerve injury and increased rapidly on the 4th day, while the expression of MAG declined on days 1–4 and reached a nadir on the 4th day (*Figure 2A*). Consistent with this, IHC showed the complete co-localization of Etv1 and S100β from day 7 after nerve injury and continued to day 28, suggesting that Etv1 expressed in SCs participated in the regulation of myelination during the post-nerve injury phase. Notably, the co-localization of Etv1 and S100β is not always observed on days 1–4 of injury (*Figure 2B*). It is well known that in the early stage of peripheral nerve injury, axons undergo degeneration and demyelination, and accordingly, SCs exhibit a transient "dedifferentiated" phenotype and are highly proliferative to help clear the myelin sheath debris. During the axon regeneration phase, SCs re-differentiate to pro-myelinating and myelinating phenotypes to form new myelin sheaths that in turn promote nerve functional recovery (37,38). Therefore, we hypothesized that the changes in Etv1 expression and cellular localization are due to the axonal demyelination and re-myelination in areas of nerve injury. Specifically, from day 7 post nerve-crush, the high expression of Etv1 and its co-localization with S100β may be due to the differentiation and myelination of SCs.

To further investigating the role of Etv1 on re-myelination, cholesterol-modified Etv1-siRNA and a negative control were injected into mouse sciatic nerves and

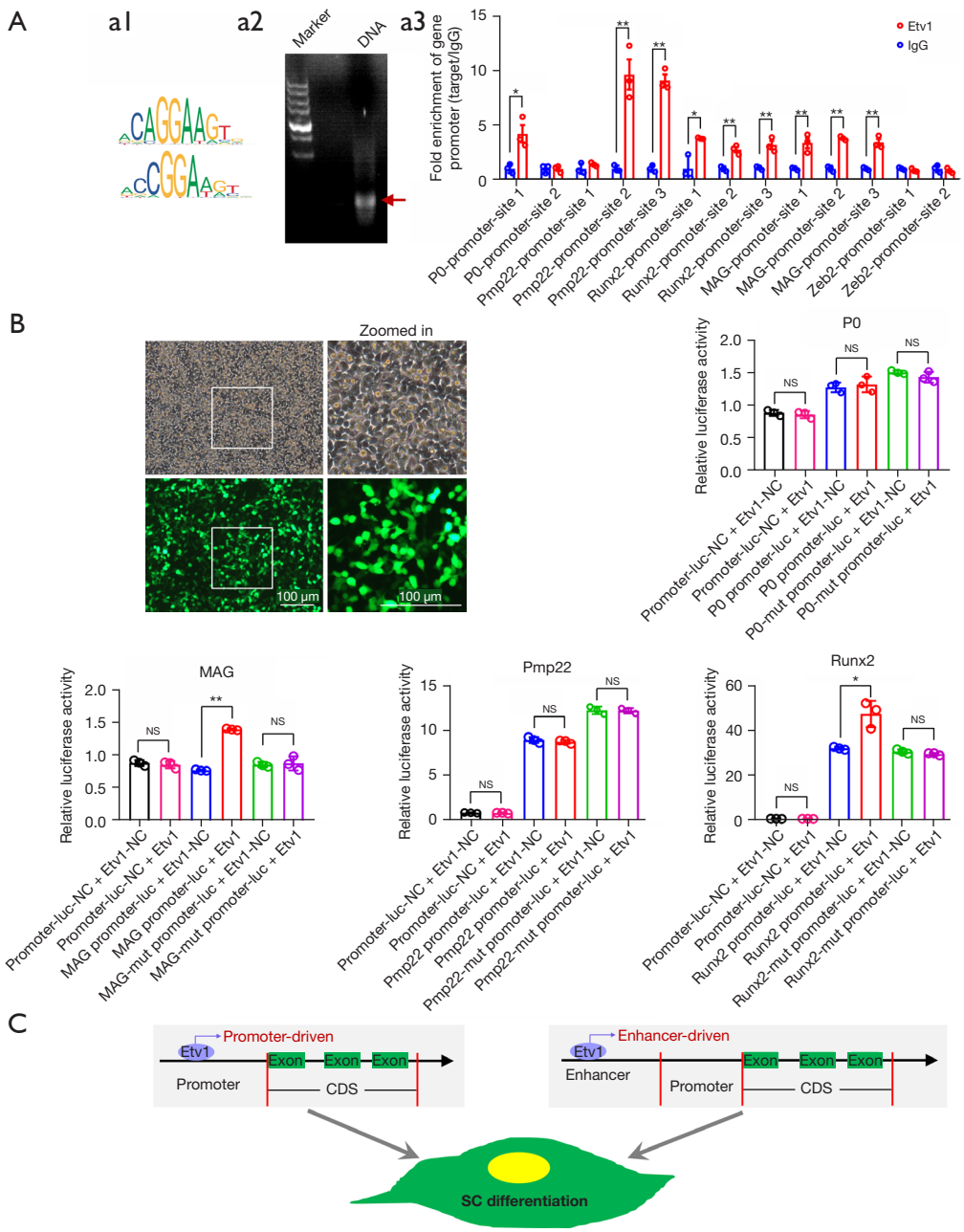

Figure 7 Etv1 recruits myelination-related genes to regulate Schwann cell differentiation. (A) The Etv1-binding regions were detected by ChIP-qPCR. (a1) Two consensus motifs at Etv1 bound sequences. (a2) A representative electropherogram showing the DNA fragments between 200 and 500 bp in lengths (red arrow). (a3) ChIP-qPCR was performed to determine the Etv1 occupancy on the P0, MAG, Pmp22, Runx2, and Zeb2 promoters in differentiating SCs. Student's *t*-test; *, P<0.05, **, P<0.01 *vs.* IgG; n=3 per group. (B) Luciferase activity of the P0, MAG, Pmp22, and Runx2 promoter, as well as a mutant promoter, in HEK293 cells co-transfected with pGV141-Etv1 (Etv1 overexpression plasmid) plus a plasmid containing the gene sequence of Renilla luciferase. The phase contrast and fluorescence images of cells after co-transfection is shown on the top left. Scale bar =100 μm. Student's *t*-test; *, P<0.05; **, P<0.01 *vs.* NC; n=3 per group. (C) A schematic diagram showing the possible mechanism by which Etv1 regulates myelination or remyelination of SCs. Etv1 may bind to the promoter or enhancer to initiate the transcription of MAG and Runx2, thereby regulating SC differentiation and myelination. NS, no statistical difference; IgG, immunoglobin G; MAG, myeline-associated glycoprotein; luc, luciferase; NC, negative control; CDS, coding sequence; ChIP-qPCR, chromatin immunoprecipitation combined with quantitative real-time PCR; SC, Schwann cell.

nerve crush injury was performed 3 days later. Assessment on day 21 post-injury revealed that Etv1 knockdown decreased SC myelination (*Figure 3* and Figure S1) and significantly reduced the number, thickness, and layer of myelin sheaths formed by the SCs. Furthermore, the ratio of myelinated/unmyelinated axons in the Etv1-knockdown nerves was significant lower than in the controls, suggesting that Etv1 may be involved in axon sorting during myelination, which is consistent with a previous report by Fleming *et al*. This latter study demonstrated that Etv1 facilitates axonal communication with non-myelinating SCs by activating the NRG1 signaling pathway, and that neurons use an independent NRG1 mechanism to interact with myelinating SCs (22). Our *in vivo* results demonstrated that MAG and Etv1 had the same expression trend during regeneration after sciatic nerve injury, and knockdown of Etv1 resulted in decreased MAG expression (*Figure 3*), further confirming that Etv1 may act as a positive regulator to promote the myelination of SCs.

Myelination of SCs is a coordinated and ordered multi-stage cellular evolution process involving multiple molecules, of which SC-lineage development is the key event. This includes directed differentiation of neural crest -derived stem cells into SC precursors, resulting in immature SCs that further proliferate, migrate, and differentiate into mature SCs (39,40). Therefore, the effect of Etv1 on specific SC behavior such as proliferation, migration, and differentiation was investigated. Furthermore, considering that myelination is closely related to the interaction between neurons and SCs, and that axons may play a role in modulating SC behavior during myelination (41), the role of Etv1 in the proliferation and migration of SCs growing on PLL and axons was examined. The results demonstrated that Etv1 knockdown in SCs inhibited their proliferation and migration, even in the presence of exogenous factors such as DRG axons (*Figures 4*,*5*). Moreover, Etv1 knockdown blocked the expression of MAG, suggesting that Etv1 is a positive regulator for myelination (*Figure 6*). The effects of Etv1 on SC behavior are consistent with the Etv1 expression dynamics during nerve injury, that is, low expression of Etv1 in SCs 1 day after injury is responsible for SC de-differentiation, and up-regulation Etv1 levels in SCs 4 days after injury would favor SC proliferation and migration. The high expression of Etv1 from days 7 to 28 post-injury is beneficial to SC differentiation and later re-myelination. Altogether, the *in vivo* and *in vitro* data suggested that Etv1 may affect myelination or re-myelination through promoting SC proliferation, migration, and differentiation.

Of interesting is the finding that Etv1 interacted with the promoters of MAG and Runx2, but not with the promoters of Zeb2, P0, and Pmp22 in differentiating SCs (*Figure 7*). MAG, P0, and Pmp22 are all constituent proteins of the myelin sheath, which are expressed by myelin-forming cells such as SCs and oligodendrocytes, and participate in myelin sheath formation and maintenance (40,42). Zeb2 and Runx2 are the key TFs involved in myelin formation, and specifically Zeb2 and Runx2 are key TFs involved in myelination, specifically implicated in SC-lineage development and differentiation in the PNS (8,43). The zinc-finger homeobox protein Zeb2 (a.k.a. Sip1 or Zfhx1) has been reported to act as a transcription repressor of several cell adhesion related genes, such as E-cadherin (44). Mice lacking Zeb2 in SCs developed severe peripheral neuropathy, and their SCs were easily dedifferentiated and became repair cells after peripheral nerve injury, but both nerve regeneration and re-myelination were disturbed, suggesting that Zeb2 inhibits myelination (45). Runx2, also known as Cbfa1, was originally identified as a multifunctional TF for osteoblast differentiation (46). Recently, Runx2 has been reported as a positive regulator involved in the regulation of SC differentiation and migration after sciatic nerve injury by activating the Akt-GSK3β signaling pathway (47,48). In the current study, ChIP-qPCR and luciferase reporter assays revealed that Etv1 targets the promoters of SC myelination genes such as MAG and Runx2, but not repressor genes such as Zeb2. Therefore, Etv1 binds to the promoters of myelinating genes, such as MAG and Runx2, to activate their transcription, thereby promoting SC differentiation and subsequent myelination. Since Etv1 also has binding sites that can intertwine with enhancers in the SC genome, it is possible that Etv1 may play a role in SC differentiation by binding to enhancers of myelin-related genes to increase their transcriptional efficiency, although this requires further investigation, such as using H3K27me3 for ChIP-seq to find the enhancer. Nonetheless, the current study demonstrated that Etv1 is a positive regulator that controls SC development and myelination by binding the promoter or enhancer region of its target gene to activate transcription (*Figure 7C*).

In conclusion, this investigation demonstrated that SC endogenous Etv1 positively regulates the ability of SCs to proliferate, migrate, and morphologically differentiate in culture or after PNS injury to facilitate myelination or re-myelination. While the binding of Etv1 to the promoter

regions of MAG and Runx2 promotes their expression, resulting in the differentiation and myelination of SCs, it is possible that there may be other gene targets that act synergistically to regulate SC myelination. Future studies are warranted to identify other specific target genes of Etv1 that affect myelination, what cues or factors they generate to regulate SC biological behavior, and to what extent these genes interact to regulate myelination. Overall, results suggested that Etv1 may serve as a potential medical target for the treatment of demyelinating diseases with future clinical applications.

Acknowledgments

Funding: This work was supported by the National Natural Science Foundation of China (No. 82001296), the National Key Research and Development Program of China (No. 2017YFA0104702), the Priority Academic Program Development of Jiangsu Higher Education Institutions (PAPD), and the "226 High-level Talent Training Project" in Nantong city.

Footnote

Reporting Checklist: The authors have completed the ARRIVE reporting checklist. Available at https://atm.amegroups.com/article/view/10.21037/atm-22-3489/rc

Data Sharing Statement: Available at https://atm.amegroups.com/article/view/10.21037/atm-22-3489/dss

Conflicts of Interest: All authors have completed the ICMJE uniform disclosure form (available at https://atm.amegroups.com/article/view/10.21037/atm-22-3489/coif). The authors have no conflicts of interest to declare.

Ethical Statement: The authors are accountable for all aspects of the work in ensuring that questions related to the accuracy or integrity of any part of the work are appropriately investigated and resolved. All experimental procedures involving laboratory animals were performed under a project license (No. S20200312-003) granted by Ethics Committee of Nantong University, in compliance with the national guidelines for the care and use of animal. A protocol was prepared before the study without registration.

References

1. Saab AS, Nave KA. Myelin dynamics: protecting and shaping neuronal functions. Curr Opin Neurobiol 2017;47:104-12.
2. Monje M. Myelin Plasticity and Nervous System Function. Annu Rev Neurosci 2018;41:61-76.
3. Pareyson D, Saveri P, Pisciotta C. New developments in Charcot-Marie-Tooth neuropathy and related diseases. Curr Opin Neurol 2017;30:471-80.
4. Miniou P, Fontes M. Therapeutic Development in Charcot Marie Tooth Type 1 Disease. Int J Mol Sci 2021;22:6755.
5. Zhou Y, Notterpek L. Promoting peripheral myelin repair. Exp Neurol 2016;283:573-80.
6. Salzer JL, Zalc B. Myelination. Curr Biol 2016;26:R971-5.
7. Villoslada P, Martinez-Lapiscina EH. Remyelination: a good neuroprotective strategy for preventing axonal degeneration? Brain 2019;142:233-6.
8. Sock E, Wegner M. Transcriptional control of myelination and remyelination. Glia 2019;67:2153-65.
9. Nave KA, Werner HB. Myelination of the nervous system: mechanisms and functions. Annu Rev Cell Dev Biol 2014;30:503-33.
10. Wegner M. Transcriptional control in myelinating glia: the basic recipe. Glia 2000;29:118-23.
11. Svaren J, Meijer D. The molecular machinery of myelin gene transcription in Schwann cells. Glia 2008;56:1541-51.
12. Stolt CC, Wegner M. Schwann cells and their transcriptional network: Evolution of key regulators of peripheral myelination. Brain Res 2016;1641:101-10.
13. Nagarajan R, Le N, Mahoney H, et al. Deciphering peripheral nerve myelination by using Schwann cell expression profiling. Proc Natl Acad Sci U S A 2002;99:8998-9003.
14. Balakrishnan A, Stykel MG, Touahri Y, et al. Temporal Analysis of Gene Expression in the Murine Schwann Cell Lineage and the Acutely Injured Postnatal Nerve. PLoS One 2016;11:e0153256.
15. Kangas SM, Ohlmeier S, Sormunen R, et al. An approach

to comprehensive genome and proteome expression analyses in Schwann cells and neurons during peripheral nerve myelin formation. J Neurochem 2016;138:830-44.
16. Zhang B, Su W, Hu J, et al. Transcriptome Analysis of Schwann Cells at Various Stages of Myelination Implicates Chromatin Regulator Sin3A in Control of Myelination Identity. Neurosci Bull 2022. [Epub ahead of print]. doi: 10.1007/s12264-022-00850-9.
17. Arber S, Ladle DR, Lin JH, et al. ETS gene Er81 controls the formation of functional connections between group Ia sensory afferents and motor neurons. Cell 2000;101:485-98.
18. Abe H, Okazawa M, Nakanishi S. The Etv1/Er81 transcription factor orchestrates activity-dependent gene regulation in the terminal maturation program of cerebellar granule cells. Proc Natl Acad Sci U S A 2011;108:12497-502.
19. Siembab VC, Gomez-Perez L, Rotterman TM, et al. Role of primary afferents in the developmental regulation of motor axon synapse numbers on Renshaw cells. J Comp Neurol 2016;524:1892-919.
20. Kandemir B, Gulfidan G, Arga KY, et al. Transcriptomic profile of Pea3 family members reveal regulatory codes for axon outgrowth and neuronal connection specificity. Sci Rep 2020;10:18162.
21. Tenney AP, Livet J, Belton T, et al. Etv1 Controls the Establishment of Non-overlapping Motor Innervation of Neighboring Facial Muscles during Development. Cell Rep 2019;29:437-452.e4.
22. Fleming MS, Li JJ, Ramos D, et al. A RET-ER81-NRG1 Signaling Pathway Drives the Development of Pacinian Corpuscles. J Neurosci 2016;36:10337-55.
23. Tao Y, Dai P, Liu Y, et al. Erbin regulates NRG1 signaling and myelination. Proc Natl Acad Sci U S A 2009;106:9477-82.
24. Lemke G. Neuregulin-1 and myelination. Sci STKE 2006;2006:pe11.
25. Newbern J, Birchmeier C. NRG1/ErbB signaling networks in Schwann cell development and myelination. Semin Cell Dev Biol 2010;21:922-8.
26. Ritchie ME, Phipson B, Wu D, et al. limma powers differential expression analyses for RNA-sequencing and microarray studies. Nucleic Acids Res 2015;43:e47.
27. Smyth GK. Linear models and empirical bayes methods for assessing differential expression in microarray experiments. Stat Appl Genet Mol Biol 2004;3:Article3.
28. Shannon P, Markiel A, Ozier O, et al. Cytoscape: a software environment for integrated models of biomolecular interaction networks. Genome Res 2003;13:2498-504.
29. Gu Y, Wu Y, Su W, et al. 17β-Estradiol Enhances Schwann Cell Differentiation via the ERβ-ERK1/2 Signaling Pathway and Promotes Remyelination in Injured Sciatic Nerves. Front Pharmacol 2018;9:1026.
30. Gu Y, Xue C, Zhu J, et al. Basic fibroblast growth factor (bFGF) facilitates differentiation of adult dorsal root ganglia-derived neural stem cells toward Schwann cells by binding to FGFR-1 through MAPK/ERK activation. J Mol Neurosci 2014;52:538-51.
31. Yamauchi J, Chan JR, Shooter EM. Neurotrophins regulate Schwann cell migration by activating divergent signaling pathways dependent on Rho GTPases. Proc Natl Acad Sci U S A 2004;101:8774-9.
32. Nawrot B, Sipa K. Chemical and structural diversity of siRNA molecules. Curr Top Med Chem 2006;6:913-25.
33. Zhao Y, Yu Y, Zhai J, et al. The Arabidopsis nucleotidyl transferase HESO1 uridylates unmethylated small RNAs to trigger their degradation. Curr Biol 2012;22:689-94.
34. Ineichen BV, Zhu K, Carlström KE. Axonal mitochondria adjust in size depending on g-ratio of surrounding myelin during homeostasis and advanced remyelination. J Neurosci Res 2021;99:793-805.
35. Pearse DD, Pereira FC, Marcillo AE, et al. cAMP and Schwann cells promote axonal growth and functional recovery after spinal cord injury. Nat Med 2004;10:610-6.
36. Monje PV, Soto J, Bacallao K, et al. Schwann cell dedifferentiation is independent of mitogenic signaling and uncoupled to proliferation: role of cAMP and JNK in the maintenance of the differentiated state. J Biol Chem 2010;285:31024-36.
37. Liu B, Xin W, Tan JR, et al. Myelin sheath structure and regeneration in peripheral nerve injury repair. Proc Natl Acad Sci U S A 2019;116:22347-52.
38. Wang JT, Medress ZA, Barres BA. Axon degeneration: molecular mechanisms of a self-destruction pathway. J Cell Biol 2012;196:7-18.
39. Jessen KR, Mirsky R. The origin and development of glial cells in peripheral nerves. Nat Rev Neurosci 2005;6:671-82.
40. Snaidero N, Simons M. Myelination at a glance. J Cell Sci 2014;127:2999-3004.
41. Osso LA, Chan JR. Architecting the myelin landscape. Curr Opin Neurobiol 2017;47:1-7.
42. Pereira JA, Lebrun-Julien F, Suter U. Molecular mechanisms regulating myelination in the peripheral nervous system. Trends Neurosci 2012;35:123-34.

43. Hung HA, Sun G, Keles S, et al. Dynamic regulation of Schwann cell enhancers after peripheral nerve injury. J Biol Chem 2015;290:6937-50.
44. Comijn J, Berx G, Vermassen P, et al. The two-handed E box binding zinc finger protein SIP1 downregulates E-cadherin and induces invasion. Mol Cell 2001;7:1267-78.
45. Quintes S, Brinkmann BG, Ebert M, et al. Zeb2 is essential for Schwann cell differentiation, myelination and nerve repair. Nat Neurosci 2016;19:1050-9.
46. Komori T. Regulation of Proliferation, Differentiation and Functions of Osteoblasts by Runx2. Int J Mol Sci 2019;20:1694.
47. Wang G, Wang Z, Gao S, et al. Curcumin enhances the proliferation and myelinization of Schwann cells through Runx2 to repair sciatic nerve injury. Neurosci Lett 2022;770:136391.
48. Ding D, Zhang P, Liu Y, et al. Runx2 was Correlated with Neurite Outgrowth and Schwann Cell Differentiation, Migration After Sciatic Nerve Crush. Neurochem Res 2018;43:2423-34.

(English Language Editor: J. Teoh)

Cite this article as: Askar P, Xu J, Hu J, Shangguan J, Sun H, Zhou S, Yang X, Chen G, Su W, Gu Y. The Etv1/Er81 transcription factor coordinates myelination-related genes to regulate Schwann cell differentiation and myelination. Ann Transl Med 2022;10(16):875. doi: 10.21037/atm-22-3489

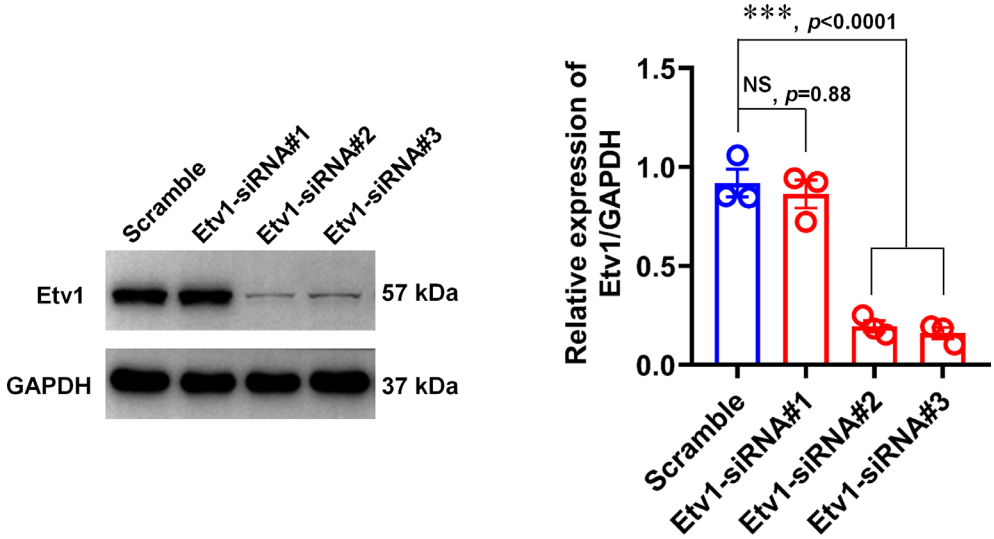

Figure S1 Validation of the Etv1-siRNAs interference efficiency. Western blots comparing Etv1 levels in SCs transfected with Etv1-siRNAs or scramble siRNA for 48 hours. The histogram shows that Etv1-siRNA significantly knocked down the expression of Etv1 in SCs. ***P<0.001 *vs.* scramble; NS, not significant; *t*-test; n=3.

https://dx.doi.org/10.21037/atm-22-3489

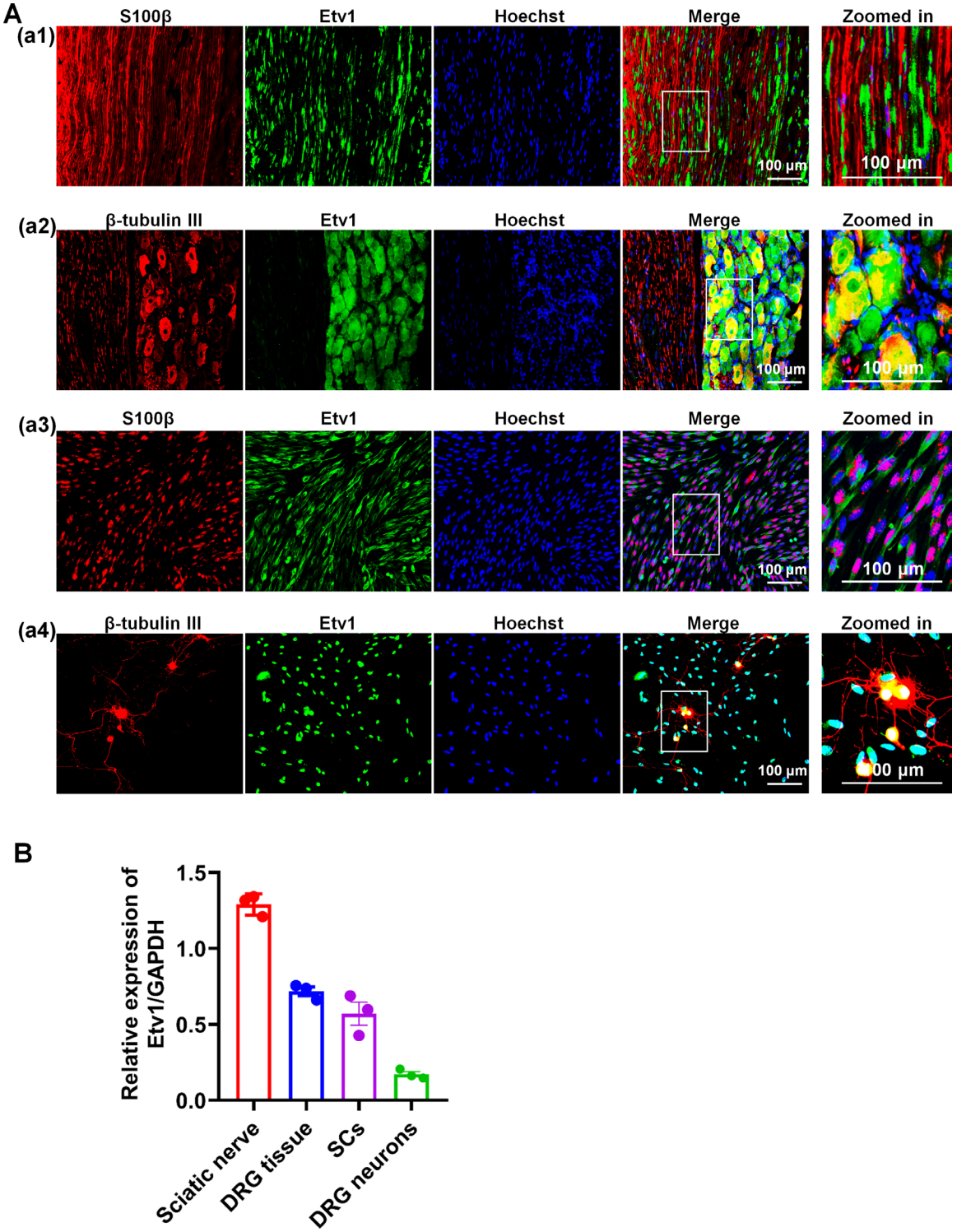

Figure S2 Etv1 expression and cell localization in PNS tissues (such as the DRG and sciatic nerves) and cells (such as SCs and DRG neurons). (A) Immunofluorescence double labeling (Etv1 and S100β or β-tubulin III) showing the expression and cell location of Etv1 in sciatic nerve (a1), DRG tissue (a2), SCs (a3), and DRG neurons co-cultured with SCs. (a4) A high magnification view of the boxed inset. Scale bar =100 μm. (B) The relative expression of Etv1 in the sciatic nerve, DRG tissue, SCs, and DRG neurons (n=3). PNS, peripheral nervous system; DRG, dorsal root ganglion; SC, Schwann cell; GAPDH, glyceraldehyde 3-phosphate dehydrogenase.

https://dx.doi.org/10.21037/atm-22-3489

Table S1 The candidate transcript factors (The maxium fold change versus 0 day >1.5)

Probset	GeneSymbol	EntrezGeneID	GeneName	Fold change 1 *d vs.* 0 d	Fold change 3 *d vs.* 0 d	Fold change 7 *d vs.* 0 d	Fold change 14 *d vs.* 0 d	Fold change 21 *d vs.* 0 d
A_44_P315647	Etv1	362733	ets variant 1	10.22608157	16.49049195	23.4403461	13.82529507	7.942571285
A_42_P655047	Prrx2	113931	paired related homeobox 2	9.207468778	7.258742811	4.324145496	13.10564179	21.18859419
A_42_P812008	Nupr1	113900	nuclear protein, transcriptional regulator, 1	5.043287836	18.6622354	8.887337237	1.75725919	3.551844857
A_44_P479890	Prrx1	266813	paired related homeobox 1	9.372981704	15.00964968	8.938065187	10.23506292	16.15703874
A_44_P509917	Isl1	64444	ISL LIM homeobox 1	3.71046629	4.871322956	12.65400062	2.8824513	7.887371339
A_43_P15106	E2f8	308607	E2F transcription factor 8	10.45196915	1.229247823	0.617011136	2.149347621	0.888850608
A_44_P353778	Foxc1	364706	forkhead box C1	4.001665563	5.689315812	8.699015892	2.635920697	2.391638488
A_44_P653701	Mybl2	296344	myeloblastosis oncogene-like 2	8.217697549	2.521846038	0.694400135	1.873763492	1.088327028
A_43_P14233	Pttg1	64193	pituitary tumor-transforming 1	5.453464339	0.960371392	0.400341478	1.301477166	1.164142232
A_44_P945456	Npas2	316351	neuronal PAS domain protein 2	1.10976548	2.470760263	5.060579964	0.765337944	0.544816311
A_42_P473594	Egr2	114090	early growth response 2	2.003437356	4.961726454	2.102116806	2.003439578	2.170147696
A_42_P762829	Cebpd	25695	CCAAT/enhancer binding protein (C/EBP), delta	1.414087115	4.464098932	3.26445088	2.303354818	3.04847842
A_44_P390700	Fhl2	63839	four and a half LIM domains 2	2.227110746	4.249408879	1.749669864	3.219811879	3.479284936
A_44_P503261	Snai2	25554	snail homolog 2 (Drosophila)	0.90674993	1.853947984	0.88067269	3.162556089	4.011932593
A_44_P448029	Rbl1	680111	retinoblastoma-like 1 (p107)	3.684228649	0.727003022	0.707588628	0.986689184	1.044733133
A_44_P348922	Cebpb	24253	CCAAT/enhancer binding protein (C/EBP), beta	2.351233251	1.509845435	1.846870658	2.470906124	3.661437239
A_42_P527141	Foxm1	58921	forkhead box M1	3.410895841	1.246347095	0.583385742	1.016843814	0.851475427
A_44_P545677	Pou3f2	29588	POU class 3 homeobox 2	1.88887941	0.587867095	3.285762643	1.087948224	1.083784761
A_44_P807777	E2f1	399489	E2F transcription factor 1	2.775142909	1.169187303	1.567317612	2.239661032	2.069334543
A_44_P184987	Myrf	293736	myelin gene regulatory factor	0.752885928	1.255694055	2.730869171	0.588193101	0.464876499
A_44_P233080	Egr1	24330	early growth response 1	2.671729656	1.661859226	1.241268253	1.568786936	1.576987983
A_44_P635089	Etv5	303828	ets variant 5	2.532124486	1.336584609	2.341740696	1.397488748	1.286663385
A_44_P386602	Brca2	360254	breast cancer 2	2.497963737	0.834872658	0.826213592	0.700108988	0.656038036
A_43_P12768	Bhlhe40	79431	basic helix-loop-helix family, member e40	1.561952232	1.187632408	1.079995674	2.026224786	2.465266933
A_44_P455160	Tfap4	360482	transcription factor AP-4	1.779406219	2.387831387	2.434163429	1.719184046	1.789613734
A_44_P164512	Stat1	25124	signal transducer and activator of transcription 1	1.323807944	2.432110145	1.964883033	1.748968574	1.577626583
A_44_P189299	Ccnd1	58919	cyclin D1	2.108242273	1.63398152	2.084190284	2.404242914	2.063693904
A_44_P367551	Sqstm1	113894	sequestosome 1	1.12324554	1.9232487	2.404054607	1.081524739	0.981275855
A_44_P330417	Twist1	85489	twist homolog 1 (Drosophila)	1.577022707	2.354686673	1.649104665	1.479090984	2.398664917
A_43_P15390	Smad7	81516	SMAD family member 7	1.505999823	0.422681625	0.544616237	1.586333311	1.731286035
A_44_P501142	Srebf1	78968	sterol regulatory element binding transcription factor 1	1.00896787	1.342064243	2.356627984	1.063928082	0.894544113
A_43_P16998	Foxo3	294515	forkhead box O3	1.062060953	2.334427095	1.397106597	1.505455886	1.592022435
A_44_P183241	Bcl6	303836	B-cell CLL/lymphoma 6	1.121521932	2.293155095	1.624348433	1.12689193	1.291116544
A_43_P19794	LOC687536	687536	similar to Forkhead box protein F1 (Forkhead-related protein FKHL5) (Forkhead-related transcription factor 1) (FREAC-1) (Hepatocyte nuclear factor 3 forkhead homolog 8) (HFH-8)	1.015830644	2.292902273	1.072084261	1.216867033	1.341492851
A_44_P395885	Cdkn2a	25163	cyclin-dependent kinase inhibitor 2A	0.983002847	1.115098897	1.133469444	2.280957132	2.075399876
A_44_P161027	Zhx2	314988	zinc fingers and homeoboxes 2	1.146695335	2.254582496	1.445815738	1.274061512	1.629671669
A_44_P313507	Cdkn2b	25164	cyclin-dependent kinase inhibitor 2B (p15, inhibits CDK4)	0.953863015	0.769950534	1.049144212	2.057851342	2.204646987
A_44_P458999	Hey2	155430	hairy/enhancer-of-split related with YRPW motif 2	1.144819195	1.287159377	2.16383861	0.892007389	0.917854429
A_44_P137334	Tfb1m	308140	transcription factor B1, mitochondrial	1.130885343	0.462367276	1.023703485	1.390738652	1.219353245
A_44_P398142	Btg2	29619	BTG family, member 2	2.124370401	1.265539906	0.888493237	0.65065842	0.940714513
A_44_P297525	Pmf1	681050	polyamine-modulated factor 1	2.113326732	1.254224002	0.829457212	1.365512323	1.030863038
A_44_P495480	Fos	314322	FBJ osteosarcoma oncogene	1.308349065	0.984336729	2.080450313	0.756942438	0.723637712
A_43_P14931	Nfe2l2	83619	nuclear factor, erythroid derived 2, like 2	1.833451157	1.612895162	2.08013765	1.71068603	1.608120298
A_44_P1030919	Nab2	314910	Ngfi-A binding protein 2	2.078123124	1.53077665	1.756314246	1.243637105	1.075386476
A_43_P13144	Cdkn2c	54238	cyclin-dependent kinase inhibitor 2C (p18, inhibits CDK4)	2.047184837	0.786457458	0.94392661	1.168886298	0.872652777
A_42_P623913	Sox18	311723	SRY (sex determining region Y)-box 18	1.004387607	2.027195977	1.23536272	1.685989089	1.384472215
A_44_P974313	Ncor1	54299	nuclear receptor co-repressor 1	1.328261067	0.498485392	1.214329775	1.215740569	1.246562139
A_44_P988451	H2afx	500987	H2A histone family, member X	2.002610708	0.632308916	0.581438255	0.908181361	0.740291362
A_44_P166749	Tfe3	317376	transcription factor binding to IGHM enhancer 3	1.114068288	0.66665627	0.91599858	0.788486413	1.965236583
A_42_P769969	Hmgn5	681284	high mobility group nucleosome binding domain 5	1.932445509	0.740986861	1.387578412	1.72864014	1.684102638
A_44_P473020	Hdac5	84580	histone deacetylase 5	0.749803969	1.928308572	0.665887286	0.86568886	0.778169172
A_44_P634946	Mdm2	314856	Mdm2 p53 binding protein homolog (mouse)	1.902306879	1.229870147	1.135088013	1.204546983	1.349742313
A_44_P481915	Id4	291023	inhibitor of DNA binding 4	1.538143566	0.660437754	1.337093636	1.900860509	1.25877855
A_44_P153979	Zeb1	25705	zinc finger E-box binding homeobox 1	0.84206739	1.888976691	1.832640491	1.213575866	1.801843279
A_42_P248193	Rel	305584	v-rel reticuloendotheliosis viral oncogene homolog (avian)	1.881702343	0.828072046	0.773169179	0.903522834	0.753065383
A_42_P541660	Nfatc4	305897	nuclear factor of activated T-cells, cytoplasmic, calcineurin-dependent 4	0.80601858	1.430306168	1.304821386	1.629164933	1.826626498
A_44_P208004	Tle4	25565	transducin-like enhancer of split 4 (E(sp1) homolog, Drosophila)	0.900635906	0.547816554	1.607988067	1.183062835	1.099021213
A_44_P327890	Tfap2c	362280	transcription factor AP-2 gamma	1.33419225	1.000768464	1.521941986	1.715382491	1.789027462
A_44_P466417	Irf2	290749	interferon regulatory factor 2	1.407045647	1.306957082	1.77603798	1.463862688	0.855884465
A_42_P693821	Fosl1	25445	fos-like antigen 1	1.772438005	1.296361577	0.993463476	1.215294111	1.245804913
A_44_P363647	Ezh2	312299	enhancer of zeste homolog 2 (Drosophila)	1.508510111	0.677453017	0.567963937	0.80919864	0.59118157
A_43_P12535	Klf10	81813	Kruppel-like factor 10	1.052409614	1.748116903	0.754953138	0.949994786	1.182493292
A_44_P277935	Arid1a	297867	AT rich interactive domain 1A (SWI-like)	1.396078921	0.57615125	0.944783822	0.908824312	0.910416851
A_43_P15648	Foxo1	84482	forkhead box O1	0.986802585	1.676893385	0.935063621	1.3101026	1.701138731
A_44_P253196	Arid5b	309728	AT rich interactive domain 5B (Mrf1 like)	1.140867674	0.589185365	1.038101469	1.207260965	1.33003287
A_43_P19663	Pax2	293992	paired box 2	1.243712937	1.688188537	1.02890506	1.347801061	1.499400685
A_44_P133449	Elf4	302811	E74-like factor 4 (ets domain transcription factor)	1.154916514	1.67937696	0.720953808	1.073858844	1.20625997
A_42_P493380	Myc	24577	myelocytomatosis oncogene	1.34020002	1.664603374	0.959848754	1.421947139	1.562157952
A_44_P195921	Psmd10	116722	proteasome (prosome, macropain) 26S subunit, non-ATPase, 10	0.96007754	1.401602254	1.600248548	1.62010614	1.640406464
A_44_P1057137	Phf1	294287	PHD finger protein 1	0.703538851	0.708270962	1.307208165	0.767569097	0.613939075
A_44_P303883	Tbx2	303398	T-box 2	1.559848953	1.359424002	1.62226162	0.714433994	0.625629335
A_43_P13702	Hexim1	498008	hexamethylene bis-acetamide inducible 1	1.112457715	0.880135569	1.599919148	0.82634282	0.616743424
A_44_P463888	Hdac4	363287	histone deacetylase 4	1.004070938	1.616901507	1.390989086	0.979938897	0.813471327
A_44_P606112	Trim24	500084	tripartite motif-containing 24	1.035737302	0.679508656	1.613743033	1.062893464	0.862969554
A_44_P439475	Klf7	363243	Kruppel-like factor 7 (ubiquitous)	1.611788562	1.02489859	1.525578235	1.401174366	1.563109666
A_44_P222030	Tbx3	353305	T-box 3	1.480302479	0.999484201	1.605711457	1.533363418	1.435309636
A_43_P12695	Ncoa2	83724	nuclear receptor coactivator 2	0.980175574	1.155067904	1.463409402	1.600324087	1.523512672
A_44_P261450	Nfkbia	25493	nuclear factor of kappa light polypeptide gene enhancer in B-cells inhibitor, alpha	1.099085027	1.59378571	1.496975213	0.894603619	0.866664591
A_44_P1057272	Ehmt2	361798	euchromatic histone lysine N-methyltransferase 2	1.134143008	0.914847746	1.592953956	1.144635746	1.025769846
A_44_P306602	Irf1	24508	interferon regulatory factor 1	1.150870097	1.516011748	1.473645658	1.590707452	1.296820588
A_44_P456752	Tp53	24842	tumor protein p53	1.006931261	1.584358591	1.000353429	1.225196315	1.12439972
A_43_P12687	Deaf1	83632	deformed epidermal autoregulatory factor 1 (Drosophila)	1.044045799	1.477371856	1.582141536	1.144124989	0.908818327
A_44_P259961	Runx2	367218	runt-related transcription factor 2	1.122174395	1.150479731	1.406197986	0.633474243	0.837437387
A_42_P620762	Atf4	79255	activating transcription factor 4 (tax-responsive enhancer element B67)	1.099012148	1.35538214	0.833517079	0.63932718	0.810705592
A_44_P297217	Sirt2	361532	sirtuin 2	0.791621207	0.988101739	1.550257103	0.965674687	0.893159146
A_44_P1027846	Cited2	114490	Cbp/p300-interacting transactivator, with Glu/Asp-rich carboxy-terminal domain, 2	0.723795478	0.944077368	1.535322609	0.66138711	0.749901319
A_43_P12423	Hif1a	29560	hypoxia-inducible factor 1, alpha subunit (basic helix-loop-helix transcription factor)	1.09561683	1.30656328	1.534370264	1.110241352	0.996283798
A_44_P536442	Phb	25344	prohibitin	0.991896504	1.53390149	1.325882106	1.257285103	1.060376669
A_44_P157222	Tgif1	316742	TGFB-induced factor homeobox 1	1.29992474	1.135700925	1.40492005	1.346999953	1.531522257
A_44_P435739	Hes1	29577	hairy and enhancer of split 1 (Drosophila)	1.451616942	1.044989346	0.762351177	1.459924437	1.504430959
A_43_P14566	Aatf	114512	apoptosis antagonizing transcription factor	0.929712677	1.504075513	1.035592915	1.022050867	0.912434562
A_44_P387246	Sin3a	363067	SIN3 homolog A, transcription regulator (yeast)	1.158454194	1.363989306	1.43505928	0.881232129	0.665374124
A_44_P391517	Nkx3-1	305999	NK3 homeobox 1	1.024124777	1.501164418	1.054676731	1.13941139	1.242045479
A_44_P166513	Atf1	315305	activating transcription factor 1	1.283449146	1.388397398	1.497495222	1.049480626	1.018220629
A_43_P22304	Casp8ap2	313128	caspase 8 associated protein 2	1.482109425	0.878238448	0.955093624	1.013041165	0.986584755
A_44_P1019537	Cbx5	300266	chromobox homolog 5	1.48200947	0.915630018	1.116501611	0.922535287	0.850703523
A_44_P280759	Npm1	25498	nucleophosmin (nucleolar phosphoprotein B23, numatrin)	1.462747244	1.37169795	1.225628004	1.32080196	1.369211834
A_42_P679251	Ascl2	24209	achaete-scute complex homolog 2 (Drosophila)	0.939107965	1.281039091	1.457038232	1.247366369	1.173353209
A_44_P177807	Epas1	29452	endothelial PAS domain protein 1	1.315248313	1.45703335	0.970888258	0.790503616	0.802328936
A_42_P734094	Notch4	406162	notch 4	1.390298437	1.26560523	0.936677165	1.451245071	1.405889916
A_44_P494130	Nfkb1	81736	nuclear factor of kappa light polypeptide gene enhancer in B-cells 1	0.886804093	1.135677204	1.439581366	1.085437758	1.141698331
A_43_P13016	Zbtb7a	117107	zinc finger and BTB domain containing 7a	1.099459148	1.117381108	1.438737938	1.095652271	1.237293702
A_44_P186860	Nfkbib	81525	nuclear factor of kappa light polypeptide gene enhancer in B-cells inhibitor, beta	0.832894498	1.243729144	1.438453582	0.901141772	0.861738473
A_44_P372529	Crem	25620	cAMP responsive element modulator	0.921789986	1.438218793	0.897729059	0.89659457	0.864494286
A_44_P224911	Wwtr1	295062	WW domain containing transcription regulator 1	1.081418543	1.232545438	1.433540337	1.109180506	0.919404416
A_44_P246114	Tle1	362533	transducin-like enhancer of split 1 (E(sp1) homolog, Drosophila)	0.881532501	1.047734854	1.430410105	0.737920056	0.773259272
A_44_P379751	Cux1	116639	cut-like homeobox 1	0.917590483	1.111989116	1.410843536	1.002814434	0.915685236
A_44_P508733	E2f3	291105	E2F transcription factor 3	1.406802009	0.862793672	1.022795298	0.932285349	0.890011655
A_42_P758492	Pitx3	29609	paired-like homeodomain 3	1.045916877	1.402946408	1.243517203	1.190940799	1.23863467
A_42_P797638	Wtip	361552	Wilms tumor 1 interacting protein	1.036066065	0.917782159	1.15548404	1.370545287	1.390908002
A_43_P22751	Mtf2	360905	metal response element binding transcription factor 2	1.300935198	0.77037456	1.030551617	0.893797553	0.719041112
A_44_P126092	Ruvbl2	292907	RuvB-like 2 (E. coli)	0.999542281	1.389774678	1.243718799	1.211962729	1.158864053
A_42_P664699	Apbb1	29722	amyloid beta (A4) precursor protein-binding, family B, member 1 (Fe65)	0.837039146	1.382360118	1.144671264	0.93945752	0.899404703
A_44_P334904	Mxi1	25701	MAX interactor 1	0.767610242	1.364596291	1.169825925	0.779083843	0.890720807
A_44_P431564	Tal1	313507	T-cell acute lymphocytic leukemia 1	0.808384557	1.349254096	0.954660143	0.98096178	1.002863022
A_44_P267809	Thoc4	690585	THO complex 4	1.345553107	0.989889001	0.835454598	1.100832778	0.897039571
A_44_P220104	Drap1	293674	Dr1 associated protein 1 (negative cofactor 2 alpha)	0.981239353	1.345077221	1.100725831	1.161631918	1.128687159
A_44_P100117	Ring1	309626	ring finger protein 1	0.847999841	1.276935718	1.34236149	1.131964777	1.139723712
A_43_P11591	Nfya	29508	nuclear transcription factor-Y alpha	1.335467068	1.032558891	0.900789261	1.186640642	1.080031906
A_43_P12125	Junb	24517	jun B proto-oncogene	1.147438051	1.154486444	1.332247384	0.944589803	1.24557892
A_44_P752074	Mef2a	309957	myocyte enhancer factor 2a	1.136556444	1.171086872	1.328648055	0.791114142	0.769318141
A_43_P21462	Pax7	500574	paired box 7	0.934530681	1.32484569	0.979662236	0.971546891	1.045305806
A_44_P550981	Dmap1	298447	DNA methyltransferase 1-associated protein 1	0.932896542	1.322016332	1.081858638	1.048280398	0.960414218
A_42_P797910	Tada3	362414	transcriptional adaptor 3	1.036548772	1.2963475	1.317339774	1.035581191	0.954533675
A_44_P137846	Tcf7l2	679869	transcription factor 7-like 2 (T-cell specific, HMG-box)	0.893121155	1.316265512	1.237680238	0.820952241	0.891588265
A_42_P788541	Pfdn5	300257	prefoldin subunit 5	0.984394157	1.201897612	1.14345189	1.250671873	1.308669685

https://dx.doi.org/10.21037/atm-22-3489

Table S2 The target gene (TR) list of 4 candidate transcript factors

TF name	TR name	TF name	TR name	TF name	TR name	TF name	TR name
Etv1	Gdap1	Egr2	Mbp	Zeb1	Mbp	Sin3a	Pmp22
	Hspb1		Pmp22		Mag		Prx
	Mtmr2		Plp1		Egr2		Egr2
	Ndrg1		Mag		Gdap1		Gdap1
	Clcn2		Prx		Nefl		Hspb8
	Pex5		Egr2		Clcn2		Hspb1
	Scn9a		Gdap1		Mars		Mtmr2
	Mars		Hspb8		Sptlc1		Nefl
	Sptlc1		Hspb1		Lmnb1		Ndrg1
	Abcd1		Nefl		Atl1		Fgd4
	Pex16		Ndrg1		Sumf1		Cnp
	Ntrk1		Cnp		Erbb3		Clcn2
	Lmnb1		Clcn2		Ugt8		Pex5
	Sumf1		Pex5		Nrg1		Scn9a
	Tf		Scn9a		Ptprz1		Pex19
	Prkca		Sacs		Prkca		Mars
	Stmn3		Abcd1		Ttc9b		Mpzl1
	Upk1b		Apoe		Atf4		Sptlc1
	Anpep		Mecp2		Egr2		Sacs
	Kifc1		Ntrk1		Nab2		Abcd1
	Atf4		Lmnb1		Nfatc4		Apoe
	Egr1		Gnao1		Sin3a		Mecp2
	Nab2		Atl1		Smad7		Pex16
	Sin3a		Nr1h3		Sqstm1		Ntrk1
	Smad7		Rtn4r		Srebf1		Lmnb1
	Sqstm1		Shank3		Tcf7l2		Gnao1
	Srebf1		Bdnf				Atl1
	Stat1		Erbb3				Sumf1
	Tf		Spp1				Snai2
			Mapt				Cryab
			Ugt8				Nf2
			Gdnf				Bdnf
			Pdgfra				D2hgdh
			Ptprz1				Pllp
			Fgf2				Erbb3
			Fgfr2				Mapt
			Tf				Ugt8
			Prkca				Plcb1
			Tac1				Cntn1
			Fgf13				Nrg1
			Ttc9b				Gpm6a
			Rasd2				Ret
			Stmn3				Pdgfra
			Apoe				Gap43
			Cdhr4				Fgf2
			Olig1				Fgfr2
			Snap25				Tf
			Hopx				Prkca
			Syp				Ttc9b
			Kifc1				Stmn3
			Atf4				Apoe
			Egr1				Eef1a2
			Egr2				Upk1b
			Id4				Snap25
			Nab2				Hopx
			Nfatc4				Syp
			Pou3f2				Kifc1
			Sin3a				Atf4
			Smad7				Egr1
			Sqstm1				Id4
			Srebf1				Nab2
			Stat1				Nfatc4
			Tcf7l2				Sin3a
			Tf				Smad7
							Sqstm1
							Srebf1
							Stat1
							Tcf7l2
							Tf

https://dx.doi.org/10.21037/atm-22-3489

Table S3 Sequences of siRNA used in RNA interference

Name	Sequence
Etv1	siRNA #1: 5'- CGTTCTCTCCGCTATTATT-3'
	siRNA #2: 5'- CAGCTTTCTGAACCCTGTA -3'
	siRNA #3: 5'- CACAGCTCATACTCCGAAA -3'

Table S4 Primers used in qRT-PCR

Name	Sequence	
Etv1	F	5'- ATCTCAGTGTTGCCAGCCTC -3'
	R	5'- AATCGAGTCACAGTAGCGGC -3'
Egr2	F	5'- AGGTTGTGCGAGGAGCAAAT -3'
	R	5'- ATTGGGGAAGATGGTCACCG -3'
Pou3f	F	5'- TCCTCAAATGCCCTAAGCCC -3'
	R	5'- CGGGAGGGGTCATCCTTTTC -3'
Myrf	F	5'- GTCATCACCAGTGGTCCCAG -3'
	R	5'- CTGGACCTGCATGGGCAC -3'
GAPDH	F	5'- GCATCTTCTTGTGCAGTGCC -3'
	R	5'- GATGGTGATGGGTTTCCCGT -3'

https://dx.doi.org/10.21037/atm-22-3489

Table S5 Primers used in ChIP-qPCR

Name		Sequence
GAPDH promoter	F	5'- CATGGGTGTGAACCATGAGA - 3'
	R	5'- GTCTTCTGGGTGGCAGTGAT - 3'
P0 (MPZ) promoter	F1	5'- TGCTGGTGACAGTTTTGTCC - 3'
	R1	5'- CCTTCCATGCATCTCAGATC - 3'
	F2	5'- CTGCATGGCAAAAGGAATC- 3'
	R2	5'- GAGATTCTACCCAGGCAGAAG- 3'
MAG promoter	F1	5'- TGGCTCAGCCACAGACTC- 3'
	R1	5'- ACACTGGTGTCACTGAGCTG- 3'
	F2	5'- CTGGCTCCGGAGTTAAGTGC- 3'
	R2	5'- CCTGGGACTCAGAGATGTC- 3'
	F3	5'- GAGGTGGTGGGGTGATTCT- 3'
	R3	5'- GTCCCAAGAGACAGGTAGAGAC- 3'
Pmp22 promoter	F1	5'- CGGATGTTAAAGGTATGCTAGG- 3'
	R1	5'- CGCTAATCTTTGCAATGGC- 3'
	F2	5'- CAGTGAGATCGTTGGTCATG- 3'
	R2	5'- GCCAGCATTCTTCAAGTCTC- 3'
	F3	5'- GCCTGTACACAGGTCAGTGT- 3'
	R3	5'- GACAGTGTCCAGCTTGTGTATC- 3'
Zeb2 promoter	F1	5'- CCCACCTACTTACGTGTTTCC- 3'
	R1	5'- GTGTGAGGGAAAGACATGG- 3'
	F2	5'- GGAAAGAGACAGTGCCTCG- 3'
	R2	5'- CCTTGGATGAAGCACACTC- 3'
Runx2 promoter	F1	5'- CTTTAGGTCAATTTGAATGACC- 3'
	R1	5'- GGATAGTAAGTAAATGCCTTCCC- 3'
	F2	5'- GACCCTAAATGAAAACTTCAGTG- 3'
	R2	5'- ATGACAAAACCACAGCAATAC- 3'
	F3	5'- CTATCCAAATCCTCATGAGTCAC- 3'
	R3	5'- TCCCTTTCTCCCTCTCTGAC- 3'

https://dx.doi.org/10.21037/atm-22-3489

Table S6 Primers used for expression vector construction in luciferase reporter assay

Name		Sequence
Etv1 (NM_001163156)	F	5'-TTTCTCTATCGATAGGTACATGGATTTTATGACCAGCAAGTG -3'
	R	5'- CTTAGATCGCAGATCTCGAGTTAGTACACGTATCCTTCGTTGT -3'
Mpz (P0) (NM_017027-promoter(-2780~86))	F	5'-TTTCTCTATCGATAGGTACCATGGAAGGAAGTGAAGTTAAGTGAGGATATTG -3'
	R	5'- CTTAGATCGCAGATCTCGAGGCTTAAAATCCCCTGGATCCCCAGCATG -3'
Mpz (P0) (NM_017027-promoter(-2780~86)-mut)	F	5'-TTCTCTATCGATAGGTACCATGGAAGGAAGTGAAGTTAAGTGAGGATATTG -3'
	R	5'-CTTAGATCGCAGATCTCGAGGCTTAAAATCCCCTGGATCCCCAGCATG -3'
MAG (NM_017190-promoter(-2130~19))	F	5'- TTTCTCTATCGATAGGTACCTTATGGGTGGGCTCCTAACC -3'
	R	5'- CTTAGATCGCAGATCTCGAGTTGGATGGTCTGGCTTCTGCGCG -3'
MAG (NM_017190-promoter(-2130~19)-mut))	F	5'- TTTCTCTATCGATAGGTACCTTATGGGTGGGCTCCTAACC -3'
	R	5'- CTTAGATCGCAGATCTCGAGTTGGATGGTCTGGCTTCTGCGCG -3'
Pmp22 (NM_017037-promoter(-1000~105))	F	5'- TTTCTCTATCGATAGGTACCTGGGACAAGTGGCCAGACTC-3'
	R	5'- CTTAGATCGCAGATCTCGAGGCCCTCCCCGCAGGACAGCGGATG -3'
Pmp22 (NM_017037-promoter(-1000~105) -mut))	F	5'- TTTCTCTATCGATAGGTACCTGGGACAAGTGGCCAGACTC-3'
	R	5'- CTTAGATCGCAGATCTCGAGGCCCTCCCCGCAGGACAGCGGATG -3'
Runx2 (NM_001278483-promoter(-2350~71))	F	5'- TTTCTCTATCGATAGGTACCGGTGGTAAAGATTATTCAAATTAAC -3'
	R	5'- CTTAGATCGCAGATCTCGAGTTGCTGTCCTCCTGGAGAAAGTTTG -3'
Runx2 (NM_001278483-promoter(-2350~71) -mut))	F	5'- TTTCTCTATCGATAGGTACCGGTGGTAAAGATTATTCAAATTAAC -3'
	R	5'- CTTAGATCGCAGATCTCGAGTTGCTGTCCTCCTGGAGAAAGTTTG -3'

https://dx.doi.org/10.21037/atm-22-3489